BIOCHEMISTRY
including biophysical chemistry & molecular biology

Article

pubs.acs.org/biochemistry

Disulfide-Mediated Stabilization of the IκB Kinase Binding Domain of NF-κB Essential Modulator (NEMO)

Li Zhou,[†] Alan T. Yeo,[‡] Carmine Ballarano,[†] Urs Weber,[‡] Karen N. Allen,*[,†] Thomas D. Gilmore,*[,‡] and Adrian Whitty*[,†]

[†]Department of Chemistry and [‡]Department of Biology, Boston University, Boston, Massachusetts 02215, United States

Supporting Information

ABSTRACT: Human NEMO (NF-κB essential modulator) is a 419 residue scaffolding protein that, together with catalytic subunits IKKα and IKKβ, forms the IκB kinase (IKK) complex, a key regulator of NF-κB pathway signaling. NEMO is an elongated homodimer comprising mostly α-helix. It has been shown that a NEMO fragment spanning residues 44−111, which contains the IKKα/β binding site, is structurally disordered in the absence of bound IKKβ. Herein we show that enforcing dimerization of $NEMO_{1-120}$ or $NEMO_{44-111}$ constructs through introduction of one or two interchain disulfide bonds, through oxidation of the native Cys54 residue and/or at position 107 through a Leu107Cys mutation, induces a stable α-helical coiled-coil structure that is preorganized to bind IKKβ with high affinity. Chemical and thermal denaturation studies showed that, in the context of a covalent dimer, the ordered structure was stabilized relative to the denatured state by up to 3 kcal/mol. A full-length NEMO-L107C protein formed covalent dimers upon treatment of mammalian cells with H_2O_2. Furthermore, NEMO-L107C bound endogenous IKKβ in A293T cells, reconstituted TNF-induced NF-κB signaling in NEMO-deficient cells, and interacted with TRAF6. Our results indicate that the IKKβ binding domain of NEMO possesses an ordered structure in the unbound state, provided that it is constrained within a dimer as is the case in the constitutively dimeric full-length NEMO protein. The stability of the NEMO coiled coil is maintained by strong interhelix interactions in the region centered on residue 54. The disulfide-linked constructs we describe herein may be useful for crystallization of NEMO's IKKβ binding domain in the absence of bound IKKβ, thereby facilitating the structural characterization of small-molecule inhibitors.

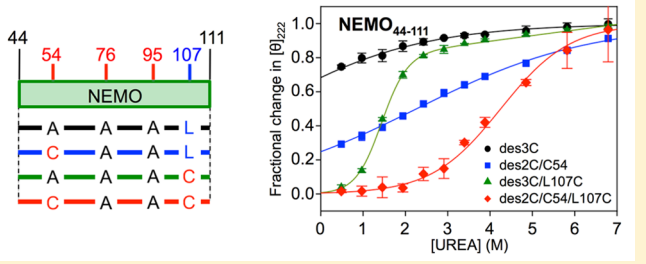

The cytoplasmic scaffolding protein NF-κB essential modulator (NEMO), also known as IκB kinase γ (IKKγ), is a compelling but also a challenging target for drug discovery.[1] In complex with the catalytic IKKα and IKKβ proteins, NEMO forms the active kinase IκB kinase (IKK), which performs a key role in activating NF-κB pathway signaling.[2] IKK phosphorylates IκB and triggers its proteolytic degradation, allowing transcription factor NF-κB to translocate to the nucleus where it modulates expression of biological effector genes.[3,4] NF-κB pathway signaling is a major regulator of many important biological processes, including cell proliferation, cell survival, and elements of the immune response, and is considered a drug target for a range of pathologies including inflammation[5] and several kinds of cancer.[6] A peptide derived from the NEMO binding domain (NBD) of IKKβ has been used in multiple studies to show that inhibition of the interaction of NEMO with IKKα/β can block cytokine-induced NF-κB activation, NF-κB-dependent gene expression and inflammation in animal models.[7−10] Thus, developing pharmaceutically useful inhibitors that bind to NEMO and block its interaction with IKKα/β is of interest as a therapeutic strategy.

Human NEMO is a 419 amino acid protein that contains five main domains: helix 1 (HLX1, sometimes called "coiled-coil 1"), helix 2 (HLX2), a coiled-coil domain (CC), a leucine zipper domain (LZ), and a C-terminal zinc finger (ZF), as illustrated in Figure 1A. Although the stoichiometry of active NEMO *in vivo* has been the subject of considerable debate,[11−14] most available data now point to a NEMO homodimer as the primary functional form of the protein.[15,16] There is strong evidence that the NEMO dimer adopts a highly extended structure,[14] and NEMO has been proposed to interact with a number of various proteins at different sites along its length.[17−19] Although no crystal structure has yet been reported for full-length NEMO, some of these interactions have been characterized in atomic detail through generation of X-ray cocrystal structures of the binding partner with a fragment of NEMO (Figure 1B).[16,20,21] In one such structure, it was shown that the NEMO binding domain of IKKβ (residues 701−745) interacts with the region of NEMO extending from approximately residues 44−111, within the

Received: July 27, 2014
Revised: October 30, 2014
Published: November 15, 2014

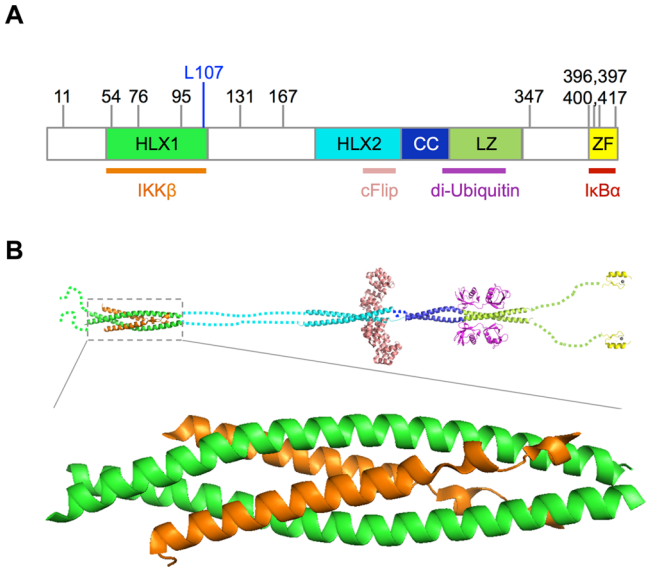

Figure 1. Domain structure of NEMO. (A) Schematic representation of the structure of human NEMO, showing the named domains helix 1 (HLX1), helix 2 (HLX2), coiled-coil (CC), leucine zipper (LZ), and zinc finger (ZF). Also shown are the locations of NEMO's 11 cysteine residues (identified by residue number above the cartoon), and of Leu107 which we mutated to cysteine in some NEMO constructs. The binding site locations for selected NEMO ligands are indicated by colored bars under the cartoon. (B) Regions of NEMO that have been characterized crystallographically: $NEMO_{44-111}$ in complex with IKKβ peptide (PDB: 3BRV);[16] $NEMO_{150-272}$ in complex with vFlip (PDB: 3CL3);[20] $NEMO_{252-336}$ in complex with diubiquitin (PDB: 2ZVN);[42] and $NEMO_{397-417}$ (PDB: 2JVX).[58] Regions for which no structure has been reported are shown as a string of dots (one dot per ~5 amino acids). Below is shown a close-up view of the 2:2 complex of $NEMO_{44-111}$ (green) with IKK$\beta_{701-745}$ (orange) from Rushe et al.[16]

helix 1 domain.[16] The structure shows that, in complex with a 44-mer peptide derived from IKKβ, $NEMO_{44-111}$ exists as an α-helical coiled coil that binds two molecules of IKKβ, one on each face of the symmetric NEMO dimer (Figure 1B). We have recently shown that interactions along the length of IKK$\beta_{701-745}$ contribute to NEMO binding. These studies confirmed and extended previous reports by showing that IKKβ residues 734–742 occupy the major binding energy hot spot on NEMO,[7] and identified two additional regions within IKK$\beta_{701-745}$ that are critical for high affinity binding to NEMO.[22]

Despite interest in the NEMO/IKKβ interaction as a drug target, several features of NEMO make drug discovery against this site challenging. As a cytoplasmic protein, NEMO is not a candidate for targeting with an antibody or other biopharmaceutical agent, and therefore must be targeted using a small-molecule (i.e., synthetic organic) drug or other drug class that is membrane permeable. Moreover, as a protein–protein interaction (PPI), the IKKβ binding site on NEMO falls into a class of drug targets that has been considered challenging for small-molecule drug discovery.[23−27] There are also obstacles to obtaining a crystal structure of NEMO or the relevant IKKβ binding domain of NEMO in an unbound state, which limits the use of structure-based approaches in any drug discovery effort. Although Rushe et al. were able to obtain a cocrystal structure of $NEMO_{44-111}$ with IKK$\beta_{701-745}$, they found that this NEMO fragment was disordered in the absence of IKKβ peptide and thus is not a good candidate for crystallization.[16] In contrast, we have recently reported evidence suggesting that residues 44–111 of NEMO are not disordered in the context of the full-length protein.[15] Nevertheless, in the absence of a means to crystallize full-length NEMO, the disorder in smaller fragments containing the IKKβ binding domain presents an obstacle to obtaining a crystal structure of this critical region of NEMO in an unbound state, or to cocrystallizing NEMO with small-molecule ligands to obtain information on their binding modes.

Here we characterize the structure and stability of the IKKβ binding domain of NEMO, and use biochemical and biophysical approaches to investigate how the active coiled-coil conformation of NEMO can be stabilized through formation of appropriately positioned interchain disulfide bonds. We demonstrate that covalent dimerization of $NEMO_{44-111}$ or $NEMO_{1-120}$, either through oxidation of the native cysteine at position 54 or by introduction of a cysteine at position 107 through a Leu107Cys mutation, induces formation of a coiled-coil structure that is stable in the absence of IKKβ peptide. We quantify the degree of stabilization afforded by interchain disulfide bonds at each of these two positions using chemical and thermal denaturation, and show that the disulfide-stabilized constructs are active for binding IKKβ. We further show that, when expressed in mammalian cells, full-length NEMO-L107C forms covalent dimers upon treatment of the cells with H_2O_2, and that NEMO-L107C can bind endogenous IKKβ and reconstitute NF-κB signaling in mammalian cells in culture. Taken together, our results show that the IKKβ binding region is natively ordered as a coiled coil within the NEMO dimer, and identify noncovalent interactions in the region of NEMO centered on Cys54 as a major contributor to coiled-coil stability. Furthermore, the disulfide-stabilized constructs we describe may enable crystallization of NEMO's IKKβ binding domain in the unbound state or with small-molecule inhibitors.

EXPERIMENTAL PROCEDURES

Construction of Bacterial and Retroviral Expression Vectors. Bacterial expression of the $NEMO_{1-120}$ and $NEMO_{44-111}$ constructs used the backbone vector pDEST-His-SUMO containing an N-terminal 9xHis-SUMO tag (Invitrogen, Carlsbad, CA). The human $NEMO_{1-120}$ or $NEMO_{44-111}$ sequence together with an N-terminal tobacco etch virus (TEV) cleavage site was cloned into this vector through two rounds of PCR using the standard Gateway cloning protocol. In the first round of PCR, the TEV cleavage site was added to the N terminus of NEMO 1–120 or 44–111 using primers containing both the TEV cleavage site and a partial NEMO sequence. A full-length human NEMO cDNA containing cysteine-to-alanine mutations at positions 11, 76, 95, 131, and 167[28] was used as a template. In the second round, attB sites were added to both ends of the first round PCR product using primers containing attB/attP sites. Primer sequences are provided in the Supporting Information. All PCRs were performed on an MJ Mini Personal Thermal Cycler (Bio-Rad) using the following conditions: 95 °C for 1 min, then 30 cycles of 95 °C for 30 s, 58 °C for 30 s, and 72 °C for 30 s, followed by 72 °C for 10 min at the completion of the cycles, and then 4 °C until the run was stopped. A total volume of 50 μL was used for PCRs, and reactions consisted of 37 μL of water, 5 μL of DeepVent thermal buffer, 1 μL of DeepVent polymerase (2.5 U/μL) (New England Biolabs), 1 μL of dNTP (10 μM), 1 μL of template (50 ng/μL), 2.5 μL of forward primer (10 μM), and 2.5 μL of reverse primer (10 μM). PCR products were purified using the QIAquick PCR Purification

Kit (Qiagen). The BP reaction was performed in a total volume of 5 μL, which included 0.4 μL of pDONR221 (375 ng/μL), 3.6 μL of PCR product (70 ng/μL), and 1 μL of Gateway BP Clonase II Enzyme mix. Samples were incubated at 25 °C for 1 h, and reactions were then quenched by adding 0.5 μL of proteinase K and incubating at 37 °C for 10 min. Products were transformed into DH5α competent cells, and colonies were isolated on LB plates containing kanamycin (50 μg/mL). Plasmids were purified from kanamycin-resistant colonies using the QIAprep Spin Miniprep Kit (Qiagen), and were sequenced to verify that the DNA sequences were inserted successfully into pDONR221. The LR reaction was then performed in a total volume of 5 μL, containing 1 μL of pDEST-His-SUMO (100 ng/μL), 2 μL of pDONR221-target DNA (125 ng/μL), 1 μL of Gateway LR Clonase II Enzyme mix, and 1 μL of water. Samples were incubated at 25 °C for 1 h, and reactions were quenched by adding 0.5 μL proteinase K and incubating at 37 °C for 10 min. Products were transformed into DH5α competent cells and transformed colonies were selected on LB plates containing ampicillin (100 μg/mL). As above, plasmids were purified by using the QIAprep Spin Miniprep Kit (Qiagen) and sequenced to verify their integrity.

Retroviral vectors (in pBABE-puro) for expression of wild-type and 7xAla NEMO have been described previously.[15] The pBABE vector for the expression of L107C was created by PCR-based overlap mutagenesis to change Leu codon 107 (CTC) to Cys (TGC) in the 7xAla NEMO mutant vector. The L107C change was confirmed by DNA sequencing. Details of retroviral vector constructions can be found at www.nf-kb.org.

Site-Directed Mutagenesis. All codon changes in bacterial expression vectors for NEMO were created using the following procedures. First, PCR using mutant oligonucleotides was performed under the following conditions: 95 °C for 1 min, then 15 cycles of 95 °C for 30 s, 55 °C for 1 min, and 68 °C for 7 min, followed by 68 °C for 10 min at the completion of the cycles, and then 4 °C until the run was stopped. Components of the PCRs were as described above. After PCR, 1 μL of DpnI was added and the samples were incubated at 37 °C for 3 h. A volume of 5 μL of the reaction was then transformed into DH5α competent cells. Plasmids with mutations were selected and sequenced as described above.

Plasmid expression vectors for the expression of FLAG-tagged 7xAla, 5xAla, and 7xAla/L107C NEMO were created by subcloning PCR-amplified cDNA fragments into pcDNA-FLAG with *Eco*RI and *Bam*HI, as described previously for wild-type pcDNA-FLAG-NEMO.[28] pcDNA-HA-TRAF6 was described previously.[29]

Protein Expression and Purification. For protein expression, plasmids were transformed into T7 express competent *Escherichia coli* BL21 (DE3) cells (New England Biolabs) according to the manufacturer's instructions, and transformants were selected on LB plates containing ampicillin (100 μg/mL). A single colony was used to inoculate 50 mL of LB with ampicillin, and the culture was incubated at 37 °C overnight with shaking. For large-scale expression, 1 L of LB containing ampicillin was inoculated with 10 mL of the overnight culture. Cells were grown at 37 °C to an OD_{600} of 0.4−0.6. To induce protein expression, IPTG was added to a final concentration of 1 mM and cells were grown for an additional 2 h. Then 2.5 g of cells were isolated by centrifugation and were lysed using a microfluidizer in 50 mL of lysis buffer containing 1 mM benzamidine, 1 mM PMSF, 0.1 mM EDTA, and 1 tablet of Roche protease inhibitor cocktail. The cell lysate was centrifuged at 18000*g* for 15 min, and the supernatant discarded, to leave a pellet containing cell debris together with inclusion bodies containing the target protein. The pellet was washed and suspended using wash buffer (lysis buffer supplemented with 0.5% Triton X-100). The washed inclusion body pellet was centrifuged as described above, and the wash step was repeated with water to remove the Triton X-100. Inclusion bodies were solubilized with 8 M Urea, by pipetting repeatedly until the inclusion bodies were thoroughly dissolved. This solubilization step can take as long as overnight to maximize the inclusion body dissolution, and to give time for full oxidation of cysteine thiols into disulfides. The denatured target protein was refolded on a HisTrap HP 5 mL column and purified. The on-column refolding and purification were performed under the following conditions: 10 mL of dissolved inclusion bodies was loaded onto the column, the bound protein was refolded by washing the column with 20 column volumes of a linear gradient of 8 M urea with nickel column binding buffer (20 mM sodium phosphate pH 7.4, 500 mM NaCl, 40 mM imidazole), and then the refolded protein was eluted from the column with elution buffer (20 mM sodium phosphate pH 7.4, 500 mM NaCl, 500 mM imidazole). Elution of the protein was monitored by UV absorbance at 280 nm, and the fractions containing protein were combined and concentrated using an Amicon Ultra-15 centrifugal filter unit according to the manufacturer's instructions. Protein was quantified by absorbance at 280 nm using a NanoDrop 2000 instrument (Thermo Scientific), using extinction coefficients calculated by the ExPASy Proteomics Server.[30]

The 9xHis-SUMO fusion partner was removed using TEV protease, as described previously.[31] Briefly, the tagged proteins were dialyzed into TEV reaction buffer (50 mM Tris-HCl pH 8.0, 0.5 mM EDTA and 1 mM DTT). TEV protease was added to the 9xHis-SUMO-NEMO substrate at a ratio of 1:100, based on $O.D._{280}$, and the reaction mixture incubated overnight at 4 °C. The product mixture was loaded onto a HisTrap HP 5 mL column to separate the untagged NEMO from the cleaved 9xHis-SUMO fusion partner. The cleaved NEMO protein was concentrated and dialyzed into 50 mM HEPES buffer. The protein was flash frozen and stored at −80 °C. All variants were analyzed by mass spectrometry to confirm the intact mass. Samples were estimated to be >95% pure as determined by SDS-PAGE. After removal of the fusion partner, the $NEMO_{44-111}$ constructs contained no tryptophan or tyrosine and, therefore, had negligible absorbance at 280 nm. For these proteins, the concentrations were measured at 205 nm in a 1 cm path length quartz cuvette, using an extinction coefficient that was calculated from the amino acid sequence as described.[32] Quantifications were performed in triplicate.

All constructs containing cysteines at position 54 and/or 107 were found to exist as 100% covalent dimer after purification, as shown by nonreducing SDS-PAGE, provided that sufficient time was allowed during solubilization of the inclusion bodies to ensure oxidation of free cysteines. For the constructs containing cysteine at both positions 54 and 107, which would migrate as a dimer in nonreducing SDS-PAGE even if only one disulfide were present, full oxidation was demonstrated using the colorimetric thiol reagent 5,5′-dithio-bis(2-nitrobenzoic acid) (DTNB). To prepare 100% monomeric forms of the cysteine-containing constructs, the protein was incubated overnight at 4 °C with 25 mM DTT in 6 M urea. The urea was removed by buffer exchange, using an Amicon column, into

a storage buffer for monomeric protein of 50 mM HEPES buffer containing 25 mM DTT.

DTT Reduction Tolerance Test. To assess each construct's tolerance to DTT, $NEMO_{1-120}$ proteins at a concentration of 100 μM were incubated in water containing 25 mM DTT at 4 °C for various periods of time, and then analyzed by SDS-PAGE without boiling. To determine whether the protein could be reduced under denaturing conditions, 100 μM of protein was incubated with 25 mM reducing agent (TCEP or DTT) with or without 6 M urea at room temperature for 1 h. Samples were then analyzed by SDS-PAGE together with a control sample that was boiled in reducing buffer containing 100 mM DTT. To determine the DTT concentration required to reduce Cys54-containing NEMO dimers under denaturing conditions, $NEMO_{1-120}$(des3C/C54) was incubated for 1 h at room temperature with 6 M urea plus various concentrations of DTT.

Circular Dichroism Spectroscopy. CD spectra were measured using an Applied Photophysics CS/2 Chirascan instrument with a 1 mm path length quartz cuvette at a scan speed of 2 nm/s. Unless otherwise indicated, spectra were measured at 10 μM NEMO protein (based on NEMO monomer) in sodium phosphate at pH 7.4 at 25 °C. The buffer background was subtracted. The measured ellipticity in millidegrees (θ) was converted to mean residue ellipticity ($[\theta]_{MRE}$) using the following equation:

$$[\theta]_{MRE} = \theta/(10Cnl) \quad (1)$$

where C is the molar concentration, n is the number of residues, and l is the path length in cm. The CD spectra in water and phosphate buffer were found to be identical, and so the results were combined and treated as replicates. Three independent measurements were conducted for each NEMO sample. The percent α-helix content was determined by comparing the $[\theta]_{MRE}$ at 222 nm measured after 2 h of incubation at room temperature in aqueous buffer (20 mM phosphate, pH 7.4) with that measured in 97% 2,2,2-trifluoroethanol (TFE), using the equation below:

$$\alpha\text{-helix}\ (\%) = \frac{\theta_{222}(\text{aqueous})}{\theta_{222}(\text{TFE})} \times 100 \quad (2)$$

Urea-Induced Denaturation Studies. NEMO protein was incubated at 25 °C for at least 1 h with freshly prepared urea solution diluted to different concentrations, in 20 mM phosphate, pH 7.4, before CD measurement of mean residue ellipticity at 222 nm as described above. Preliminary measurements showed no difference in denaturation curves when the protein was incubated for 1 or 24 h, indicating that an incubation time of 1 h was sufficient to reach equilibrium. To determine whether the denaturation was reversible, identical samples of 100 μM $NEMO_{1-120}$(des4C/L107C) were treated either with 4 M urea to ensure complete denaturation, or with water as a control. After 1 h at 25 °C, each sample was diluted 10-fold into water. After 30 min of refolding, CD spectra were taken. There was no difference between the urea treated group after refolding and water treated group (Figure S1, Supporting Information), indicating denaturation was fully reversible.

Denaturation data were fitted by nonlinear least-squares analysis to a two-state model containing additional terms to capture the effect of urea on the measured ellipticity of the fully folded and fully unfolded protein, as described.[33,34] The equation used for fitting was:

$$[\theta_{222}]_{MRE} = \frac{(y_f + m_f[\text{urea}]) + (y_u + m_u[\text{urea}])\, e^{-\left(\frac{\Delta G_{H_2O}}{RT} - \frac{m[\text{urea}]}{RT}\right)}}{1 + e^{-\left(\frac{\Delta G_{H_2O}}{RT} - \frac{m[\text{urea}]}{RT}\right)}} \quad (3)$$

where y_f and m_f are the intercept and slope of the urea dependence of $[\theta_{222}]_{MRE}$ for the fully folded protein, y_u and m_u are the corresponding intercept and slope of the fully unfolded protein, ΔG_{H_2O} is the free energy of unfolding at zero urea, m is the slope of the unfolding transition region, R is the molar gas constant, and T is absolute temperature. This model was used because the urea denaturation curves for $NEMO_{1-120}$(des4C/L107C) and for the corresponding $NEMO_{44-111}$ construct showed a positive linear slope at urea concentrations above the level required for full denaturation of the protein, indicating that in these cases urea has a small but significant effect on the ellipticity of the fully denatured protein. Fitting the denaturation curves for these constructs to the above equation while allowing m_u to have a small positive value gave a better fit to the data. For the other disulfide-stabilized constructs, allowing m_u to have a nonzero value had no significant effect on the curve fits or the values of the parameters ΔG_{H2O} or m that were obtained from the fitting; for the monomeric constructs $NEMO_{1-120}$(des4C) and $NEMO_{44-111}$(des3C), a value for m_u of ~0 was clearly preferred. In no case was a nonzero value for m_f indicated, and so this parameter was fixed at zero for all data fits. Thus, only for $NEMO_{1-120}$(des4C/L107C) and $NEMO_{44-111}$(des3C/L107C) was a pretransition or post-transition slope allowed, with a positive value for m_u being allowed in these two cases. For the monomeric constructs $NEMO_{1-120}$(des4C) and $NEMO_{44-111}$(des3C), the value of y_f, the ellipticity corresponding to fully folded protein, was poorly defined by the experimental data because the protein was <50% folded even at zero urea. Therefore, in fitting the data for these two constructs, we fixed the y_f at the mean value observed for the other three constructs in the series, based on the assumption that the fully folded state would have an α-helical content similar to that seen for the native states of the other constructs of the same length. For all denaturation experiments we found that measurements made at the lowest and highest urea concentrations (zero and 7.76 M urea) were variable and frequently anomalous, and therefore data for these extreme urea concentrations were excluded from fitting in all cases.

To linearize the denaturation data, for the purpose of more clearly illustrating the extrapolation to zero urea, we calculated the free energy of unfolding, ΔG, at each urea concentration using the following equation,

$$\Delta G = -RT \ln\left(\frac{y_f - [\theta_{222}]_{MRE}}{[\theta_{222}]_{MRE} - y_u}\right) \quad (4)$$

where the minimum and maximum ellipticities, y_f and y_u, are the values determined for each construct from the nonlinear regression analysis using eq 5. ΔG was then plotted against urea concentration to generate the linear plots.

Thermal Denaturation Studies. Proteins, at a concentration of 10 μM in 20 mM phosphate, pH 7.4, were heated from 5 to 90 °C at a rate of 2.5 °C/min, using the internal temperature control function of the CD spectrometer. Spectra from 180 to 260 nm were taken at a scanning rate of 0.5 s/nm. No obvious difference in melting curves was seen when the

dx.doi.org/10.1021/bi500920n | Biochemistry 2014, 53, 7929−7944

slower ramping rate of 1 °C/min was used, suggesting that the selected rate was appropriate. Thermal denaturation was completely reversible, as demonstrated by comparing the CD spectra $NEMO_{1-120}$(des4C/L107C) before and after thermal denaturation and refolding (Figure S2, Supporting Information). The melting temperature T_m for each protein was estimated from the maximum of a plot of the first derivative of θ_{222} was against temperature. Each result represents the average of two independent experiments.

Fluorescence Anisotropy Binding Assay. All bacterially expressed NEMO variants were characterized by measuring their binding affinities with IKKβ peptide (residues 701−745) in a direct binding format using fluorescence anisotropy (FA) as described previously.[15,22] Assays were performed in 96-well nontreated black polystyrene plates (Corning Costar), using a SpectraMax M5 microtiter plate reader (Molecular Devices, Sunnyvale, CA). For each experiment, 50 μL of water, 50 μL of 4× TNT buffer (200 mM Tris, 800 mM NaCl, 0.04% Triton X-100, 4 mM DTT, pH 7.5), 50 μL of N-terminally FITC-labeled IKKβ peptide (60 nM), and 50 μL of NEMO protein at varying concentrations were added to each well to give final concentrations of 15 nM FITC-IKKβ in 50 mM Tris, 200 mM NaCl, 0.01% Triton X-100, 1 mM DTT, pH 7.5 in a total volume of 200 μL. The plates were incubated on a plate shaker (UltraCruz shaker for microplates, Santa Cruz Biothechnology) for 1 h at 250 rpm, and were then incubated at 25 °C for 5 min before fluorescence was measured. Samples were read by excitation at 488 nm and emission at 520 nm in high sensitivity mode. Values were the averages of 100 measurements for each well, and each experiment was done in duplicate. After background subtraction the anisotropy values, A, were fitted by nonlinear least-squares regression to the modified quadratic binding equation shown below:[15]

$$A = A_0 + (A_{max} - A_0) \times \left\{ \frac{[R]_T + K_D + [L]_T - \sqrt{([R]_T + K_D + [L]_T)^2 - 4[R]_T[L]_T}}{2[L]_T} \right\} \quad (5)$$

where A_0 is the anisotropy observed for unbound FITC-IKKβ, A_{max} is the maximum anisotropy signal at saturating [NEMO], $[R]_T$ and $[L]_T$ are the total concentrations of NEMO protein and FITC-IKKβ, and K_D is the binding affinity. When fitting the binding data for the monomeric constructs $NEMO_{1-120}$(des4C) and $NEMO_{44-111}$(des3C), the value of A_{max} was fixed at the average value observed for the three disulfide-stabilized constructs in the same series.

Mammalian Cell Culture and Transfection. A293T cells and NEMO-deficient mouse fibroblasts were grown in Dulbecco's modified Eagle's medium (DMEM) (Life Technologies, Grand Island, NY) supplemented with 10% heat-inactivated fetal bovine serum (FBS; Biologos, Montgomery, IL) and penicillin−streptomycin as described.[15,28] A293T cells were transfected with plasmids for expression of FLAG-tagged NEMO or HA-tagged TRAF6 proteins using the polyethylenimine (PEI) method as described previously.[28] Retrovirus stocks for the expression of NEMO proteins were prepared by cotransfecting BOSC23 packaging cells as described previously.[15,28] After infection, retrovirally transduced NEMO-deficient fibroblasts were selected with 1 μg/mL puromycin (Sigma, St. Louis, MO).

Western Blotting and Co-Immunoprecipitation. Western blotting was performed as described previously.[15] For the analysis of FLAG-NEMO proteins from transfected A293T cells, whole-cell extracts were prepared in AT buffer (20 mM HEPES, pH 7.9, 150 mM NaCl, 1 mM EDTA, 1 mM EGTA, 20 mM $Na_4P_2O_7$, 1 mM DTT, 1% v/v Triton X-100, 20% w/v glycerol, 1 mM Na_3VO_4, 1 μg/mL PMSF, 1 μg/mL leupeptin, 1 μg/mL pepstatin). Samples containing approximately equal amounts of protein were then boiled in SDS-sample buffer (0.625 M Tris, pH 6.8, 2.3% w/v SDS, 10% w/v glycerol) with or without 5% β-mercaptoethanol. For analyzing H_2O_2-induced NEMO dimerization, transfected A293T cells were treated with 0.2 or 1 mM H_2O_2 for 10 min and samples were lysed directly in SDS sample buffer without β-mercaptoethanol. For analyzing total NEMO or phosphorylated IκBα, retrovirally transduced NEMO deficient cells were treated with 20 ng/mL TNFα (R&D Systems, Minneapolis, MN) for 10 min and then lysed directly in SDS sample buffer containing 5% β-mercaptoethanol. Samples containing approximately equal amounts of protein were then analyzed by Western blotting with anti-NEMO antiserum (#2685, Cell Signaling Technology, Danvers, MA; 1:1000 dilution) or anti-phospho-IκBα antiserum (#9246, Cell Signaling Technology; 1:1000 dilution). In all cases, the primary antibody−antigen complexes were detected with horseradish peroxidase-labeled secondary antiserum and Supersignal Dura West chemiluminescence (Thermo Scientific).

Co-immunoprecipitation experiments on transfected A293T cells were performed as described previously.[15] Briefly, cells in 35-mm tissue culture dishes were lysed in 200 μL of AT buffer. An aliquot (5 μL) was saved as the input sample. A 100 μL aliquot of the lysate was immunoprecipitated with 30 μL of anti-M2 FLAG agarose beads (cat #A2220; Sigma, St. Louis, MO). After washing, bound proteins were removed by heating the beads for 10 min at 90 °C in SDS sample buffer containing β-mercaptoethanol. Samples (input or immunoprecipitate) were then analyzed by reducing SDS-PAGE followed by Western blotting with anti-FLAG (cat #2368; Cell Signaling Technology, Danvers, MA), anti-IKKβ (sc-7607; Santa Cruz Biotechnology), or anti-HA (sc-805; Santa Cruz Biotechnology; 1:500) antiserum, as described above.

TNFα-induced Cell Death Assays. NEMO-deficient mouse fibroblasts reconstituted with 7xAla NEMO or 7xAla/L107C NEMO were treated with 50 ng/mL TNFα (R&D Systems) for 18 h, and the number of live cells was determined using a crystal violet-based cell viability assay, as described previously.[15,28]

RESULTS

Protein Design, Expression, and Purification. NEMO fragment 44−111 has previously been reported to be structurally disordered in the absence of bound IKKβ peptide.[16] Our attempts to design a stabilized form of the IKKβ binding domain of NEMO were guided by two hypotheses. One hypothesis was that a substantially longer NEMO construct, encompassing residues 1−120 would generate additional noncovalent interactions sufficient to stabilize the dimeric coiled-coil structure seen in the bound complex with IKKβ. The second hypothesis was that covalent dimerization through one or two appropriately positioned disulfide bonds would induce a stable coiled-coil. The first 120 residues of NEMO contain four cysteine residues, at positions 11, 54, 76, and 95 (Figure 1A). We have previously shown that none of these cysteines is required for the IKKβ binding activity of full-length NEMO, either *in vitro* or in cells.[15] Therefore, in designing constructs containing specific, interchain disulfide bonds, we changed all

other cysteine residues to alanine, to eliminate the possibility of disulfide-linked aggregation or non-native disulfide bonding and thereby facilitate the generation of structurally homogeneous proteins. Figure 2A shows that, of the three cysteines in the structurally characterized region of NEMO encompassing residues 44−111, Cys76 and Cys95 are positioned such that they cannot participate in interchain disulfide bonds in the IKKβ-bound conformation of the protein. Cys54, on the other hand, appears well positioned to form a disulfide bond cross-linking the two NEMO monomers that form the coiled coil

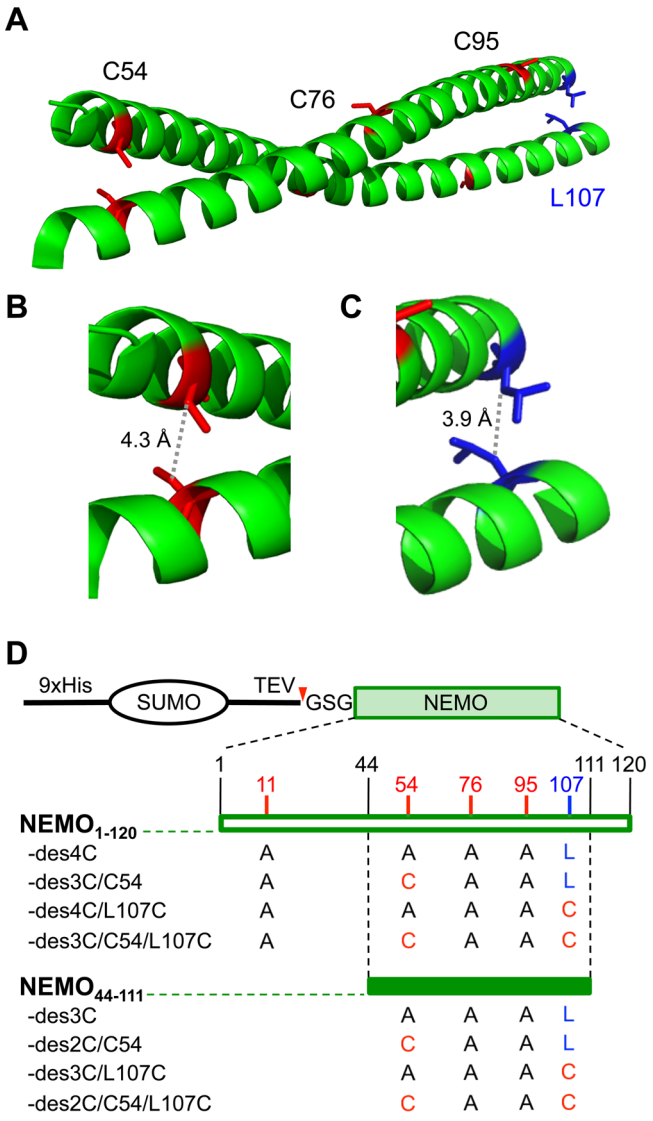

Figure 2. Design of disulfide-stabilized NEMO constructs. (A) $NEMO_{44-111}$ from the structure by Rushe et al.[16] (IKKβ peptide not shown). The locations of the cysteine residues at positions 54, 76, and 95 are highlighted in red; Leu107 is shown in blue. (B) Close-up of the region around Cys54, showing that these cysteines are well positioned to form an interchain disulfide bond. (C) Close-up of region around Leu107, showing that the β-carbons are positioned such that cysteine residues introduced through L107C mutation would be suitably positioned to form an interchain disulfide bond.[59] (D) Schematic representation of the eight NEMO constructs made in the current work. The TEV cleavage site is indicated by a red triangle. The identities of the residues present at positions 54, 76, 95, and 107 (and at position 11 for the $NEMO_{1-120}$ proteins) are indicated for each construct using the single letter code for the amino acid.

(Figure 2B). The distance between the two Cys54 β carbons is 4.3 Å, within the range of 3−6 Å required for disulfide bonds in proteins.[35] We therefore designed a construct, $NEMO_{1-120}$(des3C/C54), in which cysteines 11, 76, and 95 were changed to alanine but Cys54 was retained, to allow us to test the effect of a single interchain disulfide at position 54 on the structure and properties of $NEMO_{1-120}$, compared to a second construct, $NEMO_{1-120}$(des4C), in which all four native cysteines (11, 54, 76, and 95) were changed to alanine.

The most important region of NEMO for binding IKKβ lies roughly between residues 89 and 104,[22] some distance from Cys54. Therefore, we wished to determine whether introduction of an interchain disulfide closer to the 89−104 region would stabilize the structure of this key part of the IKKβ binding domain. Examination of the cocrystal structure of $NEMO_{44-111}$ with $IKK\beta_{701-745}$ showed that Leu107 is positioned such that mutation to cysteine should allow formation of an interchain disulfide bond with minimal disruption of the polypeptide backbone conformation (Figure 2C). We therefore made a third construct, $NEMO_{1-120}$(des4C/L107C), in which all four native cysteines were changed to alanine, and a cysteine was introduced at position 107. Finally, we created a fourth construct that contained both the native Cys54 and the L107C mutation, designated $NEMO_{1-120}$(des3C/C54/L107C), to test the effect of interchain disulfide bonds at both of these positions on the structure and stability of $NEMO_{1-120}$. The structures of these four $NEMO_{1-120}$ constructs are shown schematically in Figure 2D. To enable us to distinguish effects due to construct length from effects due to the introduction of interchain disulfide bonds, we created a corresponding set of mutants based on the minimal IKKβ binding region $NEMO_{44-111}$, designated $NEMO_{44-111}$(des3C), $NEMO_{44-111}$(des2C/C54), $NEMO_{44-111}$(des3C/L107C), and $NEMO_{44-111}$(des2C/C54/L107C) (Figure 2D).

The NEMO constructs described above were expressed in bacteria as SUMO fusion proteins containing an N-terminal 9xHis tag for affinity purification and a tobacco etch virus (TEV) cleavage site between the SUMO domain and the first NEMO residue (Figure 2D). The SUMO fusion partner was used to improve expression and to provide additional bulk to facilitate analysis of NEMO protein binding properties by fluorescence anisotropy (FA). The TEV site was designed such that removal of the 9xHis-SUMO fusion partner with TEV protease left only three non-native amino acids (Gly-Ser-Gly) at the N terminus of the NEMO protein. The proteins were expressed in *E. coli*, resolubilized from inclusion bodies under denaturing conditions in 8 M urea, and refolded on a Ni/NTA metal ion affinity column before being eluted from the column with an imidazole gradient. Analysis of the products by SDS-PAGE showed that, with the exception of $NEMO_{1-120}$(des4C) and $NEMO_{44-111}$ (des3C) which contain no cysteines, all constructs purified as covalent dimers, and could be reduced to monomers of the expected size by boiling in 100 mM DTT for 5 min (Figure 3A). The 9xHis-SUMO fusion partner was removed by incubation of the purified fusion constructs with TEV protease, followed by removal of the cleaved 9xHis-SUMO fragment by passage over a Ni/NTA metal ion affinity column, as described in Experimental Procedures (Figure 3B−D). Notably, constructs containing Cys54 were highly resistant to reduction under native conditions. For example, treatment of the cleaved $NEMO_{1-120}$(des3C/C54) with 25 mM DTT at 4 °C achieved only ∼50% reduction even after 3 weeks

dx.doi.org/10.1021/bi500920n | *Biochemistry* 2014, 53, 7929−7944

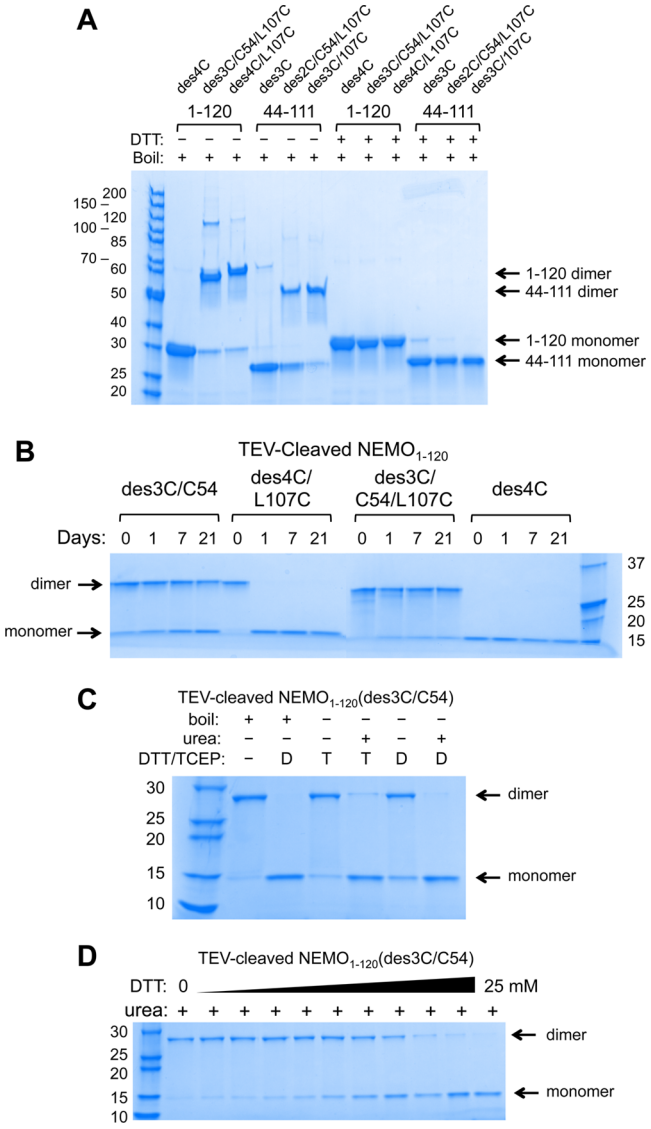

Figure 3. Analysis of NEMO constructs by SDS-PAGE. (A) SDS-PAGE analysis showing that $NEMO_{1-120}$(des4C) and $NEMO_{44-111}$(des3C) purify as monomers, while the other cysteine containing $NEMO_{1-120}$ and $NEMO_{44-111}$ constructs as isolated are predominantly covalent dimers that can be reduced to monomers by boiling under reducing, denaturing conditions. (B) Susceptibility of the $NEMO_{1-120}$ proteins to reduction with 25 mM DTT after removal of the 9xHis-SUMO fusion partner using TEV protease. The cleaved products were treated with 25 mM DTT in water at 4 °C for various times, and then analyzed by SDS-PAGE without boiling. The C54 containing constructs are highly resistant to reduction under nondenaturing conditions, whereas the construct containing only a single disulfide at position 107 is readily reduced. The result shown is representative of two independent experiments. (C) SDS-PAGE analysis showing that TEV-cleaved $NEMO_{1-120}$(des3C/C54) can be reduced by 25 mM DTT or TCEP (1 h at room temperature) under denaturing conditions. (D) SDS-PAGE analysis (without boiling) of TEV-cleaved $NEMO_{1-120}$(des3C/C54) incubated with various concentrations of DTT, decreasing from 25 mM in 2-fold dilutions, in 6 M urea for 1 h at room temperature, showing that 25 mM DTT is required to reduce $NEMO_{1-120}$(des3C/C54) even under denaturing conditions.

(Figure 3B), with $NEMO_{1-120}$(des3C/C54/L107C) showing even less reduction under similar conditions. Either boiling or denaturant (urea) was required in addition to DTT to completely reduce the dimer (Figure 3C). Even under denaturing conditions, 25 mM DTT or TCEP was required to reduce Cys54-containing constructs within 1 h (Figure 3D). In contrast, $NEMO_{1-120}$(L107C) was readily reduced by DTT even in the absence of urea (Figure 3B).

Introduction of Interchain Disulfides Induces Increased α-Helical Structure in NEMO. To test the hypothesis that the NEMO N-terminal domain α-helical coiled-coil can be stabilized by the inclusion of all residues from 1 to 120 or by covalent dimerization through appropriately placed disulfides, we characterized the structure and stability of the eight NEMO constructs shown in Figure 2D using circular dichroism (CD) spectrometry, after removal of the 9xHis-SUMO tag with TEV protease. The α-helical content was quantified by comparison to the spectrum obtained for the same construct in 97% 2,2,2-trifluoroethanol (TFE), a solvent which favors α-helix formation,[36,37] as shown in Figure S3 (Supporting Information). Fully reduced, monomeric $NEMO_{1-120}$(des3C/C54) gave a CD spectrum indicating only 37% α-helical structure (Figure 4A), identical to the helical content of $NEMO_{1-120}$(des4C) which contains no cysteines (Table 1). These values are similar to the 32% α-helical content seen with the monomeric construct $NEMO_{44-111}$(des3C) (Table 1), suggesting that extension of this shorter fragment to include residues 1−43 and 112−120 was not sufficient to stabilize a coiled-coil structure. In contrast, CD analysis of the same construct in the oxidized state, which is a covalent dimer due to an interchain disulfide bond at position 54, showed a substantial increase in α-helical content to 60% (Figure 4A). $NEMO_{1-120}$ containing an engineered interchain disulfide at position 107 ($NEMO_{1-120}$(des4C/L107C)) or containing disulfides at both positions 54 and 107 ($NEMO_{1-120}$(des3C/C54/L107C)) similarly showed 60−70% α-helical content (Table 1). In the shorter $NEMO_{44-111}$ constructs, the presence of disulfide bonds at positions 54 and/or 107 increased α-helical content to an even greater degree, with the values ranging from 75 to 88% α-helix depending on the construct (Figures S3 and S4, Supporting Information and Table 1).

In the published X-ray crystal structure of $NEMO_{44-111}$ with $IKK\beta_{701-745}$, amino acids 44−48 and 111 are not visible in the structure, suggesting that these terminal residues are substantially disordered or mobile. The residual GSG tripeptide left at the N termini of our constructs after TEV cleavage presumably also is disordered. Thus, for the $NEMO_{44-111}$ constructs adoption of the conformation seen in the crystal structure would correspond to 60 residues of α-helix out of 70 residues total = 86% α-helix content. Thus, the level of α-helix content observed for the three disulfide-stabilized $NEMO_{44-111}$ constructs, shown in Table 1, is consistent with the nearly complete adoption of the active conformation of the protein that was seen crystallographically.[16] For the longer $NEMO_{1-120}$ constructs, adoption of a fully α-helical structure between residues 50 and 108, with the remainder of the protein being disordered, would correspond to an α-helix content of 49% (60 out of 123 residues). The extent of α-helix content observed for the disulfide-stabilized forms of $NEMO_{1-120}$ thus indicates that an additional dozen or so of the ∼60 residues outside the immediate $IKK\beta$ binding region are also α-helical in these constructs. This interpretation is consistent with the observation that a fraction of $NEMO_{1-120}$(des4C) spontaneously adopts an α-helical structure even as a monomer. Taken together, the above results show that enforcing covalent dimerization via an interchain disulfide bond at position 54

dx.doi.org/10.1021/bi500920n | Biochemistry 2014, 53, 7929−7944

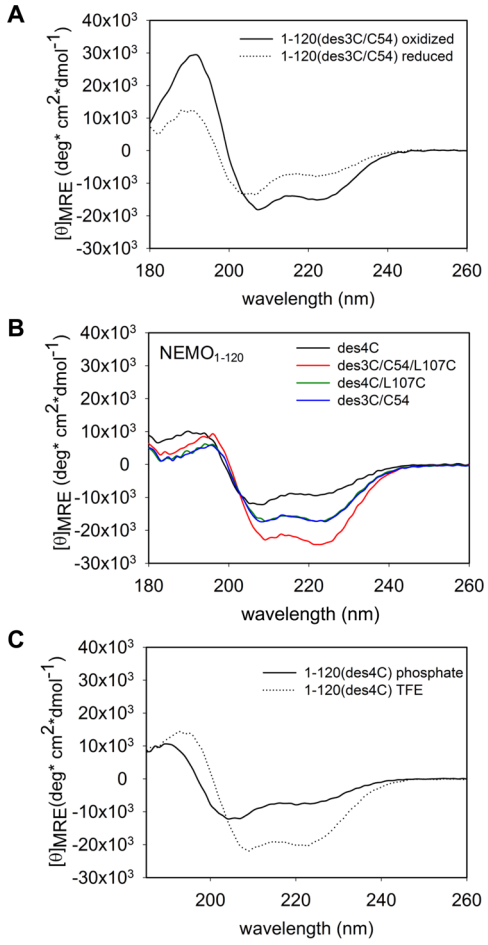

Figure 4. Effect of interchain disulfide bonds on NEMO secondary structure. (A) Overlaid CD spectra in 20 mM phosphate, pH 7.4, showing that fully reduced, monomeric TEV-cleaved NEMO$_{1-120}$(des3C/C54) possesses only modest α-helix content (dotted line), whereas the oxidized form of the same construct, containing an interchain disulfide bond at position 54, possesses a substantially α-helical structure (solid line). Spectra shown are representative of two independent experiments. (B) Overlaid CD spectra (20 mM phosphate, pH 7.4) showing the relative α-helical content of the four TEV-cleaved NEMO$_{1-120}$ constructs shown in Figure 2D. NEMO$_{1-120}$(des3C/C54) (blue), NEMO$_{1-120}$(des4C/L107C) (green) and NEMO$_{1-120}$(des3C/C54/L107C) (red) are present in their oxidized, covalent dimer forms. The spectrum of the monomeric NEMO$_{1-120}$(des4C) is shown in black. Spectra shown are representative of three independent experiments. Corresponding data for the NEMO$_{44-111}$ constructs are shown in Figure S4 (Supporting Information). (C) CD spectra showing that NEMO$_{1-120}$(des4C), which in aqueous buffer is largely disordered (solid line), adopts an α−helical structure in 97% TFE (dotted line). Spectra shown are representative of two independent experiments. Spectra for all eight constructs are shown in Figure S3, and the measured values for mean residue ellipticity at 222 nm are provided in Table S1 (Supporting Information).

and/or position 107 stabilizes a conformation of NEMO that is largely α-helical in the IKKβ binding region extending roughly from residues 50−108, but that the protein outside of this region remains largely unstructured especially in the longer, NEMO$_{1-120}$ constructs.

Disulfide-Stabilized NEMO Constructs Show Increased Binding Affinity for IKKβ. To determine whether the increased α-helical content of the disulfide-stabilized NEMO constructs described above is due to stabilization of the active α-helical coiled-coil conformation seen crystallographically for NEMO$_{44-111}$ bound to IKK$\beta_{701-745}$ peptide,[16] we tested the ability of each protein to bind FITC-labeled IKK$\beta_{701-745}$. FITC-IKK$\beta_{701-745}$ has been shown previously to bind to both full-length NEMO[22] and to truncated NEMO constructs that contain the NEMO N-terminal domain.[16] For these measurements, we used the FA binding assay that we have described previously.[22] In this assay, a fixed concentration of 15 nM FITC-IKK$\beta_{701-745}$ is incubated with various concentrations of NEMO protein. The binding affinity can be determined by plotting total anisotropy versus NEMO concentration and fitting to the appropriate quadratic or hyperbolic binding equation.[15,38] We used the intact 9xHis-SUMO fusion proteins for these initial measurements to maximize the reduction in tumbling rate of the labeled peptide upon binding, so as to ensure a robust change in anisotropy.

We initially measured the binding of FITC-IKK$\beta_{701-745}$ to the four NEMO$_{1-120}$ constructs. We also compared the binding activity of NEMO$_{1-120}$(des3C/C54) as a covalent dimer versus as a fully reduced monomer, so as to directly test the consequences for activity of the presence or absence of an interchain disulfide bond in the same construct. The results show that the monomeric forms of NEMO$_{1-120}$ bound IKK$\beta_{701-745}$ with only micromolar affinity, but the forms stabilized by interchain disulfide bonds at positions 54 and/or 107 bound 6−30-fold more strongly (Figure 5A, Table 1). A similar pattern of activities was seen for the NEMO$_{44-111}$ constructs des3C, des3C/L107C, and des2C/C54/L107C (des2C/C54 was not tested) (Figure S5A, Supporting Information). To make sure that the binding activities of the constructs were not influenced by the presence of the 9xHis-SUMO we repeated the measurements with the NEMO$_{1-120}$ constructs after removal of the fusion partner. The results showed that the presence of the fusion partner had no significant effect on the binding properties of the constructs (Figure S5B, Supporting Information). Taken together, these results indicate that the disulfide-stabilized forms of NEMO are active, and that covalent dimerization preorganizes the polypeptide in a conformation that confers relatively high affinity binding with IKKβ.

Interchain Disulfide Bonds Increase the Resistance of NEMO to Chemical and Thermal Denaturation. To assess the effect of covalent dimerization on the stability of the α-helical structure of NEMO, we performed chemical and thermal denaturation experiments on the NEMO constructs using CD to monitor loss of secondary structure. A decrease in mean residue ellipticity at 222 nm (θ_{222}) indicates a decrease in α-helical content.[39] These measurements were done using the TEV-cleaved NEMO constructs to avoid interference from the presence of the 9xHis-SUMO fusion partner. Preliminary time-course measurements showed that the extent of denaturation attained its equilibrium value within 1 h, leading us to choose an incubation period of 1 h for subsequent experiments. As shown in Figure 5B, all four NEMO$_{1-120}$ constructs were completely denatured by 8 M urea at 25 °C. However, at lower concentrations of urea they showed different degrees of denaturation. NEMO$_{1-120}$(des4C), which contains no cysteine and thus cannot form covalent dimers, was highly sensitive to denaturant. Indeed, the CD analysis showed that NEMO$_{1-120}$(des4C) is <50% ordered even in the absence of urea. NEMO$_{1-120}$(des3C/C54) and NEMO$_{1-120}$(des4C/L107C) showed $[\text{urea}]_{50}$ values of 1.5−2.0 M, indicating that the

dx.doi.org/10.1021/bi500920n | Biochemistry 2014, 53, 7929−7944

Table 1. Structure, Stability, and Binding Affinities of the NEMO Constructs from Figure 2D

NEMO variant	α-helix (%)[a]	$[urea]_{50}$ (M)[b]	slope (m) (cal/M)[b]	ΔG_{H_2O} (kcal/mol)[c]	T_m (°C)[d]	K_D (nM) tagged[e]	K_D (nM) untagged[f]
$NEMO_{1-120}$							
des4C	37 ± 5	<0	330 ± 20	−0.2 ± 0.02	27 ± 2	1.900 ± 100	1500 ± 400
des3C/C54[g]	60 ± 1	1.9 ± 0.9	390 ± 60	0.7 ± 0.2	33 ± 2	70 ± 9	120 ± 70
des4C/L107C[g]	61 ± 7	1.5 ± 0.3	1500 ± 130	2.3 ± 0.2	45 ± 2	310 ± 30	240 ± 90
des3C/C54/L107C[g]	72 ± 8	4.3 ± 0.5	720 ± 40	3.0 ± 0.2	67 ± 4	180 ± 20	80 ± 40
$NEMO_{44-111}$							
des3C	32 ± 3	<0	320 ± 20	−0.4 ± 0.02	24 ± 2	5600 ± 240	n.d.[h]
des2C/C54[g]	75 ± 4	2.3 ± 0.9	290 ± 40	0.6 ± 0.2	34 ± 3	n.d.	n.d.
des3C/L107C[g]	88 ± 23	1.4 ± 0.2	1900 ± 110	2.7 ± 0.2	43 ± 2	210 ± 20	n.d.
des2C/C54/L107C[g]	83 ± 15	4.2 ± 0.8	670 ± 70	2.8 ± 0.2	70 ± 2	560 ± 50	n.d.

[a]Percent α-helix content, determined by comparing CD spectra measured in aqueous buffer versus in 97% TFE. Values are the average ± SD from three independent experiments. [b]Concentration of urea required to give 50% denaturation at 25 °C, and slope value (m) for the denaturation curve, determined through nonlinear regression analysis of urea denaturation curves measured in three independent experiments. Errors are standard errors from the fit of the averaged data. [c]Free energy of unfolding extrapolated to [urea] = 0 M, determined through nonlinear regression analysis of urea denaturation curves measured in three independent experiments. Errors are standard errors from the fit of the averaged data. [d]Melting temperature, determined from CD melting curves. Values are the average T_m from two independent experiments ± the larger of half the difference or 2 degrees. [e]Affinity for binding to FITC-IKK$\beta_{701-745}$, measured by fluorescence anisotropy using the 9xHis-SUMU-tagged constructs. Values are the best fit for a single experiment performed in duplicate; errors are the Standard Errors for the curve fits. [f]Affinity for binding to FITC-IKK$\beta_{701-745}$, measured by fluorescence anisotropy using the untagged $NEMO_{1-120}$ constructs generated by removal of the fusion partner using TEV protease. Values are the best fit for averaged data from three independent experiments; errors are the standard errors for the curve fits of the averaged data. [g]Covalent dimers due to interchain disulfide bond(s) at positions 54 and/or 107. [h]n.d.: Not done.

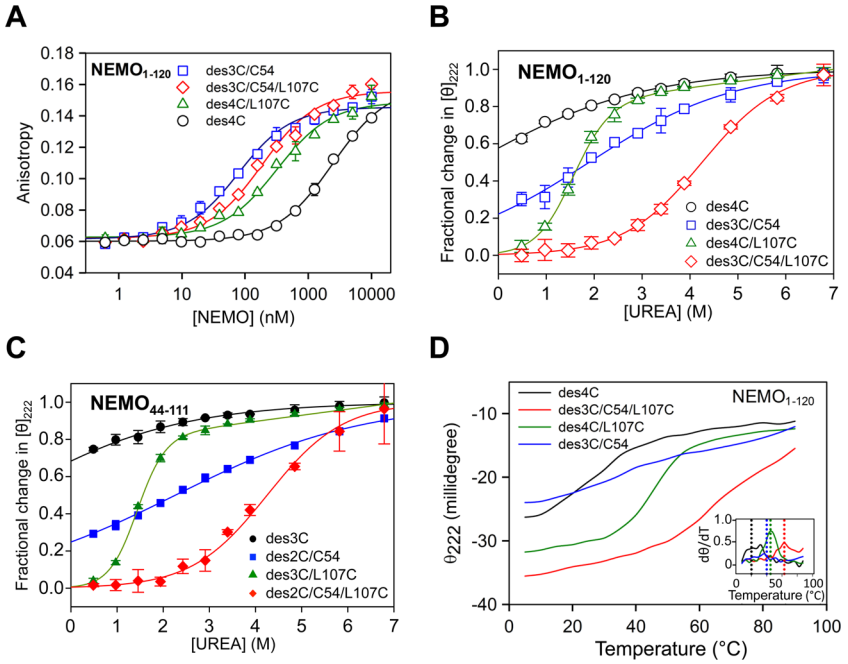

Figure 5. Structural stability and binding affinity for IKKβ. (A) Binding affinity of the 9xHis-SUMO-tagged $NEMO_{1-120}$(des4C) (black circles), -(des3C/C54) (blue squares), -(des4C/L107C) (green triangles), and -(des3C/C54/L107C) (red lozenges) for FITC-IKK$\beta_{701-745}$, measured by fluorescence anisotropy. The solid lines represent the best fit to a quadratic binding equation, as described in Experimental Procedures. Results show the averages of duplicate measurements, with the error bars showing the spread between the duplicate values. The corresponding data for the tagged $NEMO_{44-111}$ constructs are shown in Figure S5A, and for the TEV-cleaved $NEMO_{1-120}$ constructs in Figure S5B (Supporting Information). (B,C) Urea denaturation curves for the TEV-cleaved $NEMO_{1-120}$ constructs and $NEMO_{44-111}$ constructs, respectively, as measured by CD (20 mM phosphate, pH 7.4). The solid lines represent the best fit to a two-state denaturation equation, as described in Experimental Procedures. The curve fits for $NEMO_{1-120}$(des4C/L107C) and $NEMO_{44-111}$(des3C/L107C) contain an extra term to account for the effect of urea on the observed ellipticity of the fully denatured protein (see text). Plotted are average values from three independent experiments; error bars are standard deviations. The $[urea]_{50}$, slope (m), and ΔG_u values obtained from the curve fits are collected in Table 1. (D) Thermal denaturation of the TEV-cleaved $NEMO_{1-120}$ constructs, monitored by the change in θ_{222} measured by CD (in 20 mM phosphate, pH 7.4). Colors are as in (A). Inset shows the first derivative of the melting curve to illustrate how T_m was determined. Data shown are representative of two independent experiments. The corresponding data for the $NEMO_{44-111}$ constructs are shown in Figure S7 (Supporting Information). In panels (A)−(D) the cysteine-containing constructs are present in their oxidized, covalently dimeric form.

dx.doi.org/10.1021/bi500920n | Biochemistry 2014, 53, 7929−7944

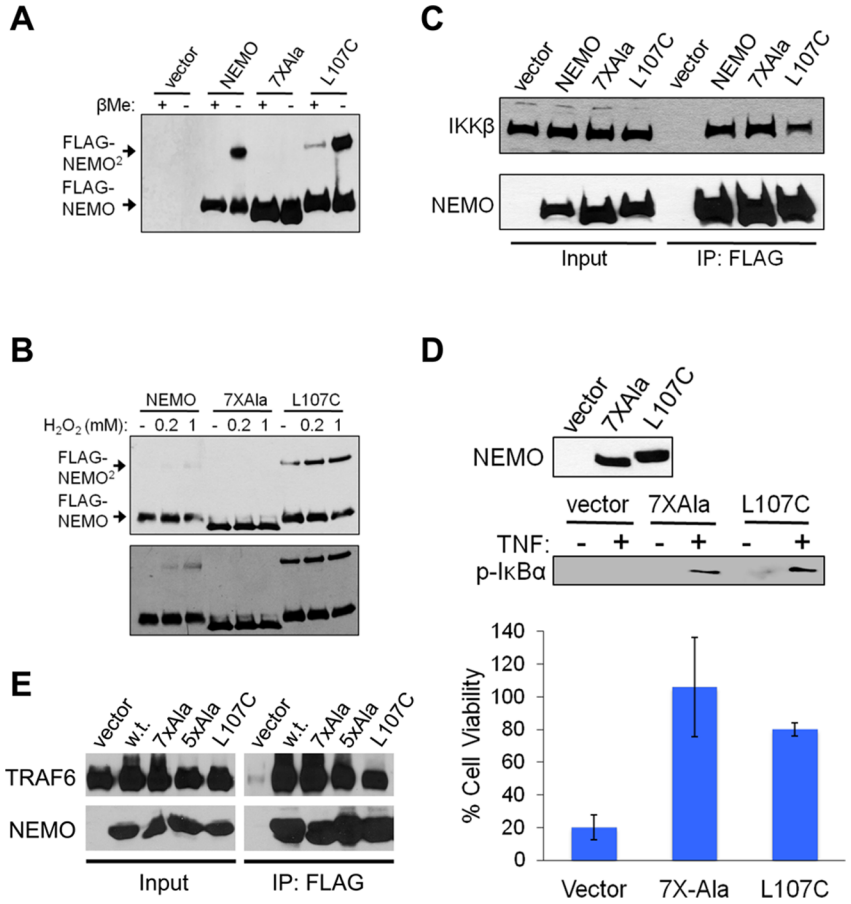

Figure 6. Activity of full-length NEMO-L107C *in vivo*. A293T cells were transfected with expression vectors for the indicated FLAG-tagged NEMO proteins or an empty vector (A–C). (A) Whole-cell extracts were prepared in AT buffer and samples were boiled in the presence (+) or absence (−) of β-mercaptoethanol (βMe). Samples were then analyzed by anti-FLAG Western blotting. The positions of FLAG-NEMO monomers and dimers (FLAG-NEMO^2) are indicated. (B) Cells were treated with the indicated concentrations of H_2O_2 for 10 min and whole-cell extracts were prepared directly in SDS-sample buffer lacking βMe. Western blotting was then performed as in (A). Shorter (top) and longer (bottom) exposures of the same blot are shown to allow for visualization of the increase in L107C dimer with H_2O_2 treatment (upper image) and the dose-dependent dimerization of wild-type NEMO (bottom image). (C) Extracts from cells transfected with the indicated FLAG-tagged NEMO proteins were immunoprecipitated with anti-FLAG beads (IP: FLAG) and then Western blotted for either IKKβ (top) or FLAG-NEMO (bottom). The lanes marked Input include 5% of the extract used in the immunoprecipitation. (D) NEMO-deficient mouse fibroblasts were transduced with retroviral vectors for the indicated NEMO proteins or the corresponding empty vector. To confirm NEMO protein expression, extracts were subjected to anti-NEMO Western blotting (top panel). Cells were also treated (+) with 20 ng/mL of TNFα for 10 min and extracts were subjected to Western blotting for phospho-IκBα (middle panel). For the bottom graph, cells were treated with 50 ng/mL TNFα for approximately 18 h, and the number of viable cells was quantified by crystal violet staining. % Cell Viability is percentage of viable cells after TNFα treatment as compared to the parallel, untreated cultures. Values are the averages of three experiments performed with triplicate samples, with the indicated standard deviations. (E) A293T cells were cotransfected with expression vectors for HA-TRAF6 and for the indicated FLAG-tagged NEMO proteins or an empty vector. The identity of the NEMO constructs is as follows: w.t., wild-type NEMO; 7xAla, NEMO in which the seven cysteine residues at positions 11, 54, 76, 95, 131, 167, and 347 have each been mutated to Ala; 5xAla, NEMO in which the five cysteine residues at positions 11, 76, 95, 131, and 167 are mutated to Ala, such that Cys54 and Cys347 are retained; L107C, 7xAla NEMO in which the additional mutation L107C has been introduced. The 7xAla and 5xAla NEMO constructs have been described previously.[15] Extracts from cells were immunoprecipitated with anti-FLAG beads (IP: FLAG) and then Western blotted for either HA-TRAF6 (top) or FLAG-NEMO (bottom). The identity of the HA-TRAF6 protein was confirmed by anti-TRAF6 Western blotting [not shown]. The lanes marked Input include ~5% of the extract used in the immunoprecipitation.

presence of a single interchain disulfide bond at position 54 substantially stabilized the protein. The presence of two disulfides, at 54 and 107, resulted in additional stabilization, as shown by NEMO$_{1-120}$(des3C/C54/L107C) which gave a [urea]$_{50}$ value of 4.3 ± 0.5 M. In comparing the denaturation curves for NEMO$_{1-120}$(des3C/C54) and NEMO$_{1-120}$(des4C/L107C), it is notable that the construct containing the engineered Cys107 has a much steeper slope than that containing only the native Cys54.

We analyzed the urea denaturation curves to determine the free energy of unfolding of each variant extrapolated to zero urea, ΔG_{H_2O}, by fitting the results to a two-state unfolding model (eq 3, Experimental Procedures) using nonlinear regression (Figure 5B).[33,34] This analysis is valid only if denaturation is reversible. We therefore tested reversibility by incubating NEMO$_{1-120}$(des4C/L107C) in 4 M urea for 1 h, conditions which fully denature this construct (Figure 5B), and then diluting the protein 10-fold into aqueous buffer to give a final urea concentration of 0.4 M. The CD spectrum of the renatured protein was indistinguishable from that of a protein sample that was treated identically in the absence of urea (Figure S1, Supporting Information), showing that urea

dx.doi.org/10.1021/bi500920n | *Biochemistry* 2014, 53, 7929–7944

denaturation of the protein was fully reversible. Analysis of the denaturation curves showed that the monomeric $NEMO_{1-120}$ construct containing no cysteines is largely denatured even in the absence of urea, with $\Delta G_{H_2O} < 0$ at 25 °C (Table 1). The presence of a single interchain disulfide at position 54 stabilized the folded state to give $\Delta G_{H_2O} = 0.7 \pm 0.2$ kcal/mol, while the engineered disulfide at position 107 achieved a greater stabilization of 2.3 ± 0.2 kcal/mol. The $NEMO_{1-120}$ construct containing disulfides at both 54 and 107 was the most stable, with $\Delta G_{H_2O} = 3.0 \pm 0.2$ kcal/mol. The denaturation behavior of the $NEMO_{44-111}$ constructs was essentially identical to that seen for the longer NEMO constructs, both qualitatively (Figure 5C) and quantitatively (Table 1). The denaturation data for the $NEMO_{1-120}$ and $NEMO_{44-111}$ were also plotted in a linearized form, as shown in Figure S6 (Supporting Information), and showed good linearity, further validating the use of a two-state unfolding model.

We also characterized the stability of the NEMO variants in response to thermal denaturation. We monitored the structure of each protein by CD using ellipticity at 222 nm measured while slowly increasing the temperature of the sample from 5 to 90 °C. As shown in Figure 5D, the NEMO 1−120 variants showed a range of melting temperatures. $NEMO_{1-120}$(des4C) gave a melting temperature of $T_m = 27 \pm 2$ °C, consistent with this monomeric construct being <50% structured at room temperature. The presence of a single disulfide at either position 54 or 107 substantially stabilized the proteins, resulting in T_m values of 33 and 45 °C, respectively. The construct containing two disulfides was highly stable to thermal denaturation, melting only at 67 ± 4 °C. The thermal stabilities of the $NEMO_{44-111}$ constructs were also measured, and gave similar results to those seen with the longer $NEMO_{1-120}$ proteins (Table 1 and Figure S4, Supporting Information).

The L107C Mutation Can Mediate Covalent Dimerization of Full-Length NEMO, and Does Not Affect NEMO's Ability to Activate NF-κB Signaling and Bind to TRAF6 in Cells. We have previously shown that Cys54 can engage in interchain disulfide bonding to form a covalent NEMO dimer in the context of full-length NEMO protein,[15,28] but that the presence or absence of a disulfide at Cys54 does not affect the binding affinity for IKKβ because full-length NEMO is constitutively dimeric even when fully reduced *in vivo*.[15] The structural and functional consequences of introducing a cysteine at position 107 into full-length NEMO have not previously been investigated, however. To gain additional evidence that the L107C mutation we introduced into the $NEMO_{1-120}$ and $NEMO_{44-111}$ constructs does not compromise the protein's function, we introduced the L107C change into full-length NEMO and evaluated the activity of this construct in a range of cellular assays. The L107C change was made in the 7xAla NEMO background to allow us to evaluate disulfide formation at position 107 without interference from the cysteines present in wild-type protein at positions 54 and 347, which can mediate covalent dimerization of NEMO *in vivo*.[15,28] We have previously shown that the 7xAla NEMO mutant can fully restore NF-κB signaling when expressed in NEMO-deficient mouse fibroblasts.[15] First, we determined whether a cysteine at position 107 can mediate interchain disulfide bond formation in full-length NEMO in cells. FLAG-tagged versions of wild-type, 7xAla, and 7xAla/L107C NEMO were expressed in A293T cells and the protein's propensity to form disulfide mediated dimers was assessed in two ways: (1) by the formation of dimers post-lysis in the presence of molecular oxygen, and (2) by the formation of dimers when intact cells were treated with hydrogen peroxide. We have shown previously that exposure of cell lysates to molecular oxygen can induce NEMO dimer formation in a Cys54/347-dependent fashion.[28] Therefore, we lysed cells overexpressing the relevant NEMO proteins under oxidizing conditions and then analyzed NEMO protein by Western blotting under reducing (plus β-mercaptoethanol) or nonreducing (no β-mercaptoethanol) conditions. As shown in Figure 6A, wild-type NEMO and 7xAla/L107C NEMO (but not 7xAla NEMO) were converted to covalent dimers when cells were lysed under these nonreducing conditions, and these dimers were reduced to monomers by treatment of the lysates with SDS sample buffer containing β-mercaptoethanol before SDS-PAGE. Similarly, treatment of intact cells with H_2O_2 induced wild-type and 7xAla/L107C NEMO, but not 7xAla NEMO, to form covalent dimers (Figure 6B). Indeed, we generally found that the L107C mutant formed disulfide-bonded dimers more efficiently than wild-type NEMO under both conditions.

To assess the ability of L107C NEMO to participate in NF-κB signaling, we conducted three experiments. First, by coimmunoprecipitation using anti-FLAG beads, we found that overexpressed FLAG-7xAla/L107C NEMO could interact with endogenous IKKβ in A293T cells, as could FLAG-tagged wild-type and 7xAla NEMO (Figure 6C). Second, NEMO-deficient fibroblasts were retrovirally transduced with 7xAla or 7xAla/L107C NEMO, or a control vector containing no gene. Cells were then treated with TNFα for 10 min to measure phosphorylation of IκBα or for 18 h to assess the ability of the given NEMO protein to protect cells from TNFα-induced cell death. Cells expressing either 7xAla or 7xAla/L107C NEMO showed an increase in phospho-IκBα in response to 10 min treatment with TNFα (Figure 6D, middle), whereas control cells showed no phospho-IκBα in the presence or absence of TNFα. Moreover, 7xAla NEMO and 7xAla/L107C NEMO both restored the ability of the NEMO-deficient cells to survive when treated with TNFα for 18 h, whereas transduction with an empty retroviral vector did not protect these cells (Figure 6D, bottom). Activation of the NF-κB pathway in response to TNFα requires that NEMO interact not only with IKKβ through its N-terminal domain, but also with IκB through NEMO's C-terminal zinc finger domains[40,41] and (non-covalently) with di-Ubiquitin through NEMO's central CoZi domain.[42] NEMO has also been shown to interact with E3 ligase TRAF6 for activation of a variety of downstream signaling pathways that are important for normal cell function, and several human disease mutations specifically affect the NEMO-TRAF6 interaction.[43,44] Therefore, as an additional measure of NEMO activity, we assessed the ability of our Cys mutant NEMO proteins to interact with TRAF6. As shown in Figure 6E, all NEMO Cys mutants (7xAla, 5xAla [7xAla + C54/347], and 7xAla/L107C) interacted with TRAF6 as efficiently as wild-type NEMO, as measured by coimunoprecipitation from transfected A293T cells. Thus, the functional assay shown in Figure 6D provides evidence that 7xAla/L107C NEMO retains the ability to productively interact with key binding partners at sites up and down its length.

Taken together, these results demonstrate that a cysteine at residue 107 of NEMO can participate in disulfide formation in the context of full-length NEMO when expressed in mammalian cells, and that the L107C mutation does not affect the ability of NEMO to functionally interact with IKKβ, IκB,

dx.doi.org/10.1021/bi500920n | *Biochemistry* 2014, 53, 7929−7944

diubiquitin or TRAF6 or to activate productive NF-κB signaling in mammalian cells.

DISCUSSION

In this work we tested the hypothesis that the N-terminal domain of NEMO possesses a stable coiled-coil structure in the dimeric state, where dimer formation is induced either by the introduction of interchain disulfide bonds or by noncovalent interactions between NEMO polypeptides of sufficient length. The results show that enforcing dimerization through one or two appropriately positioned disulfide bonds results in essentially full ordering of the α-helical coiled-coil region between approximately residues 50 and 108, which constitutes the IKKβ binding region of NEMO. This induced ordering preorganizes this region of NEMO for binding IKKβ, as shown by the accompanying enhancement in IKKβ binding affinity. In contrast, NEMO residues 1−50 appear to be largely disordered in both bound and unbound states. The finding that enforcing dimerization of the NEMO IKKβ binding domain induces a stable α-helical coiled coil supports our previous proposal that the IKKβ binding region of NEMO is ordered in the context of the full-length protein, which is constitutively dimeric.[15]

An interesting feature of our findings is that the presence of an interchain disulfide bond at position 54 versus position 107 appears to stabilize the active, coiled-coil conformation of NEMO to different extents. Constructs containing a single disulfide at position 54 were relatively easy to denature, but were exceptionally difficult to reduce, whereas constructs containing a single disulfide at position 107 were more difficult to denature but easier to reduce. The resistance to reduction of NEMO molecules containing Cys54 suggests that a disulfide at this position is buried within a relatively extensive and intimate contact interface, thereby restricting access by the reducing agent. Examination of the published X-ray crystal structure of $NEMO_{44-111}$ in complex with $IKK\beta_{701-745}$ indicates that the interaction between the NEMO polypeptides is close and relatively extensive in the vicinity of Cys54, as compared to the much less intimate contact in the region of Leu107 (Figure 7).[16] There is minimal direct interaction between the NEMO monomers outside of these two localized contacts (Figure 7C). The greater free energy of unfolding with $NEMO_{1-120}$(des4C/L107C) and $NEMO_{44-111}$(des3C/L107C), compared to the constructs containing only a disulfide at Cys54, is consistent with this interpretation. Denaturation of the constructs containing a single disulfide at position 107 involves disruption of the intimate contact between the NEMO monomers in the vicinity of amino acid 54, while the presence of a disulfide at position 54 presumably locks this region together such that denaturation involves primarily the disruption of only the weaker interaction around Leu107. This interpretation also accounts for the different slopes of the urea denaturation curves for the constructs with a single disulfide at position 107 versus position 54. According to the widely used Transfer Model for protein denaturation,[45] the degree of cooperativity observed in chemical denaturation experiments, represented by the slope factor m in eq 3, reflects the extent to which the solvent-exposed surface area of the protein increases upon denaturation.[46,47] Thus, the large slopes seen for the proteins containing only a disulfide at 107 indicates that denaturation is accompanied by a large increase in solvent-exposed surface area relative to the other constructs. We therefore conclude that the difference in denaturation behavior and ease of reduction between the NEMO constructs containing a single disulfide at position 54 versus 107 derives from a close and favorable contact between NEMO monomers in the region centered on residue 54, which remains strong even when Cys54 is changed to alanine. The large denaturation energy seen in the construct containing disulfides at both of these positions likely has a

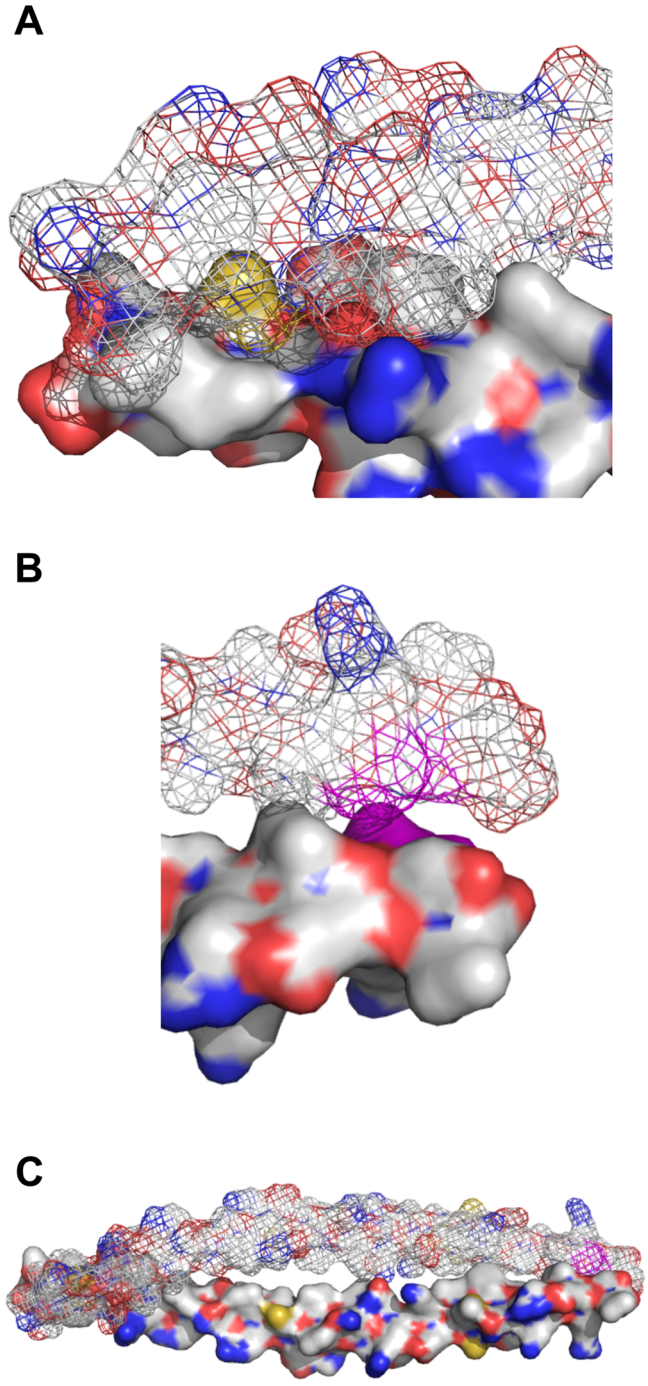

Figure 7. Regions of contact at the NEMO−NEMO interface, from the published cocrystal structure of $NEMO_{44-111}$ in complex with IKKβ(701−745) (PDB code 3BRV).[16] (A) Cys54 (colored yellow) is largely buried at the center of an extensive and intimate contact interface between the two NEMO monomers, one of which is shown in surface representation and the other as a wire-frame. (B) Much poorer contact is apparent in the vicinity L107 (colored magenta). (C) Corresponding representation of the whole of $NEMO_{44-111}$, showing that the regions shown in panels (A) and (C) represent the only points of direct contact in this domain of the NEMO dimer.

dx.doi.org/10.1021/bi500920n | Biochemistry 2014, 53, 7929−7944

different explanation, presumably reflecting the fact that the denatured state in a doubly cross-linked NEMO dimer is highly constrained and compact, and benefits from only a fraction of the entropy gain that accompanies denaturation of the singly cross-linked forms. Note that full-length NEMO, though constitutively dimeric, does not have interchain disulfides in the normal reducing environment of the cell[15,28] and, therefore, the presence of a cysteine that can be oxidized at position 54 to form a disulfide in the dimer interface is unlikely to play a major role in NEMO function under normal cellular conditions.

Our results additionally provide quantitative insight into the energetics of coiled-coil formation in the IKKβ binding domain of NEMO, as illustrated in Figure 8. The binding of monomeric $NEMO_{44-111}$(des3C) to IKKβ can notionally be separated into two steps: (1) association of two disordered monomers to form an ordered noncovalent coiled-coil dimer, with free energy $\Delta G_{Dimeriz}$, and (2) binding of two IKKβ molecules to this noncovalent dimer to form the final complex. The self-association of NEMO monomers can be further subdivided into three notional steps. 1(a) Colocalization of the monomers into close proximity, with an energetic cost equal to the configurational entropy cost of colocalizing two molecules from a 1 M standard state such that their translational and overall rotational motions are coupled (ΔS_{Config}). 1(b) Adoption of a fully α-helical structure separately by each monomer, with an energy cost for each corresponding to the inverse of the free energy of unfolding, ΔG_{H_2O}, for $NEMO_{44-111}$(des3C). 1(c) Interaction of the two α-helical monomers to form a noncovalent, coiled-coil dimer, with the release of interaction energy $\Delta G_{Interact}$. If the hypothetical preorganized noncovalent $NEMO_{44-111}$ dimer is assumed to bind IKKβ with a similar affinity to that observed for the disulfide-stabilized $NEMO_{44-111}$ covalent dimers, then the 20-fold difference in IKKβ binding affinity between dimer (step 2) and monomer (labeled as step 3 in Figure 8) implies that $\Delta G_{Dimeriz}$ is small ($-RT\ln 20$ = 1.8 kcal/mol). Given that ΔS_{Config} is known to be a large number (6−12 kcal/mol[48−53]) and ΔG_{H_2O} is negative, the noncovalent interaction energy between $NEMO_{44-111}$ monomers, $\Delta G_{Interact}$, must be considerable. Specifically, to account for the 6−30-fold difference in IKKβ binding affinity, the NEMO monomers must interact sufficiently strongly that approximately (1/30)−(1/6) = ∼3−15% of the NEMO protein exists as dimer at the concentration of 0.1−1 μM at which binding is seen in our assays. Thus, even the relatively small NEMO fragments we use here appear to show some tendency to preassociate, presumably mediated by close and energetically favorable contacts in the vicinity of residue 54. The interaction affinity is low, however, and therefore under the conditions of our experiments the constructs lacking any interchain disulfide bonds are largely monomeric, consistent with the previously published NMR data for $NEMO_{44-111}$.[16] The ∼35% α-helix content we observed with these constructs therefore presumably reflects mostly adventitious helix formation within a monomeric polypeptide. The observation that the shorter $NEMO_{44-111}$(des3C) binds IKKβ approximately as strongly as the longer $NEMO_{1-120}$(des4C) confirms that regions outside residues 44−111 do not significantly contribute to NEMO self-association or to IKKβ peptide binding. The energy diagram for the longer, $NEMO_{1-120}$ constructs should therefore look essentially identical to that shown in Figure 8, as the additional residues present in these longer constructs do not contribute to IKKβ binding and remain largely disordered even in the bound state.

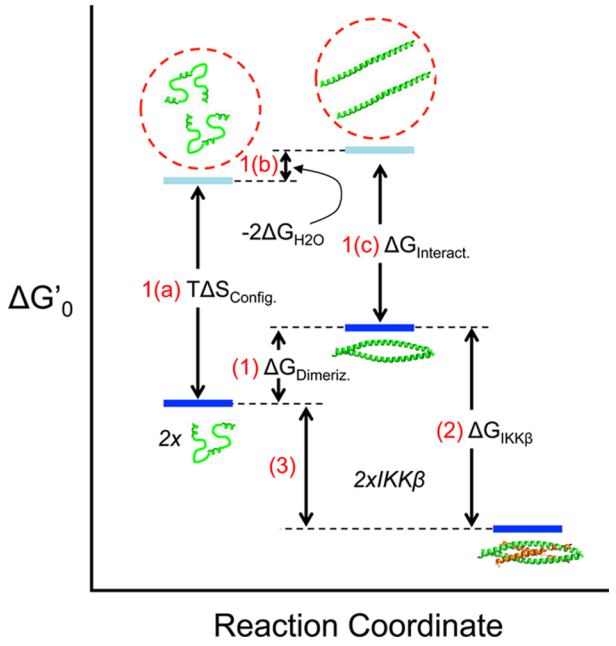

Figure 8. Energetic relationship between NEMO−NEMO interaction and coiled-coil formation in $NEMO_{44-111}$. The binding of monomeric $NEMO_{44-111}$(des3C) to IKKβ can notionally be separated into two steps: (1) association of two disordered monomers to form an ordered noncovalent coiled-coil dimer, with free energy $\Delta G_{Dimeriz}$, and (2) binding of two IKKβ molecules to this noncovalent dimer to form the final complex. The self-association of NEMO monomers can be further subdivided into three notional steps. 1(a) colocalization of the monomers into close proximity (represented by a dashed red circle), where ΔS_{Config} is the configurational entropy cost of colocalizing two molecules from a 1 M standard state such that their translational and overall rotational motions are coupled. 1(b) adoption of a fully α-helical structure separately by each monomer, with an energy cost for each corresponding to the inverse of the free energy of unfolding, ΔG_{H_2O}, for $NEMO_{44-111}$(des3C). 1(c) Interaction of the two α-helical monomers to form a noncovalent, coiled-coil dimer, with the release of interaction energy $\Delta G_{Interact}$. If the hypothetical preorganized noncovalent $NEMO_{44-111}$ dimer is assumed to bind IKKβ with a similar affinity to that observed for the disulfide-stabilized $NEMO_{44-111}$ covalent dimers, then the 20-fold difference in IKKβ binding affinity between dimer (Step 2) and monomer (Step 3) implies that $\Delta G_{Dimeriz}$ is small ($-RT\ln 20$ = 1.8 kcal/mol). Given that ΔS_{Config} is known to be a large number (6−12 kcal/mol, see text) and ΔG_{H_2O} is negative, the noncovalent interaction energy between $NEMO_{44-111}$ monomers, $\Delta G_{Interact}$, must be considerable. The energy diagram for the longer, $NEMO_{1-120}$ constructs would look essentially identical to that shown here, as the additional residues present in these longer constructs do not contribute to IKKβ binding and remain largely disordered even in the bound state.

Although a wide range of values have been reported for the binding affinity of NEMO for IKKβ,[15,16,22,54,55] studies using full-length NEMO in conjunction with $IKK\beta_{701-745}$ peptide indicate an affinity for this interaction in the single digit nanomolar range.[22] It is noteworthy that even our disulfide-stabilized, constitutively dimeric N-terminal domain constructs of NEMO showed affinities that are ∼10-fold larger than that observed for the full-length protein. There are several possible reasons for this difference. It is unlikely that the lower affinity results from the Cys-to-Ala changes at positions 76 or 95, because we have previously shown that these changes in full-length NEMO do not affect binding affinity for $IKK\beta_{701-745}$.[15]

dx.doi.org/10.1021/bi500920n | Biochemistry 2014, 53, 7929−7944

However, one possibility is that, notwithstanding our careful selection of the disulfide locations, the positioning of the disulfides in our constructs is not fully compatible with high affinity binding of IKKβ. We consider this explanation unlikely, however, for two reasons. We have previously shown that oxidation of Cys54 does not affect the binding affinity of full-length NEMO for IKKβ,[15] and we show here that introduction of the L107C mutation into full-length NEMO did not affect its ability to bind IKKβ, IκB, diubiquitin, or TRAF6 or to mediate TNFα-induced activation of NF-κB in cells. Furthermore, the ability of the full-length NEMO 7xAla/L107C protein to form a covalent dimer upon treatment of cells with H_2O_2 supports our hypothesis that these residues are appropriately positioned in the native structure to form an interchain disulfide bond. Moreover, it is unlikely that attenuation of IKKβ binding affinity of such similar magnitude would occur with two disulfides at such different locations within the NEMO structure. Nevertheless, even small differences in structure resulting in conformational or dynamic constraints on the NEMO structure could account for a difference in binding affinity of the magnitude that we observed, and therefore, we cannot rule out this possibility. An alternative explanation for the discrepancy in binding affinities between our constructs and full-length NEMO is that regions of the NEMO sequence downstream of the N-terminal 120 residues are required for maximal IKKβ binding affinity.

One practical consequence of our results is to enable the identification of forms of the NEMO N-terminal domain that would be amenable to crystallization in the unbound state, or cocrystallization with small molecules identified in screens for inhibitors of the IKKβ binding site on NEMO.[56] In the absence of conditions for crystallizing full-length NEMO or larger fragments that contain the IKKβ binding domain, cocrystallizing compounds with only the IKKβ binding region itself, as was done with IKK$\beta_{701-745}$,[16] would appear to be the best option. However, the high degree of disorder that these workers demonstrated for the NEMO$_{44-111}$ in the absence of IKKβ peptide suggested that crystallization of unbound NEMO$_{44-111}$ would not be possible. Nor is it likely that a weak-binding small molecule occupying a small portion of the IKKβ binding site would stabilize an ordered NEMO structure in the same way that the 45-mer IKKβ peptide does. Our results show that the IKKβ binding region of NEMO can be induced to adopt a stable coiled-coil structure in the absence of ligand, by introduction of an interchain disulfide bond at position 54 and/or position 107, and that the resulting, rigidified proteins are compatible with IKKβ binding and NF-κB signaling *in vivo*. Given the large number of single amino acid changes along the length of NEMO that are associated with human disease,[57] we find it surprising that a NEMO protein with eight scattered amino acid changes (as in L107C)) retains normal activity. However, we have only looked at the ability of the 7xAla and L107C NEMO mutant proteins to support signaling to NF-κB in response to TNFα, and to bind to TRAF6. Therefore, we cannot rule out the possibility that other activities are defective in these NEMO mutants.

Our results also suggest that the regions of NEMO between approximately residues 1 and 44 are disordered in our NEMO$_{1-120}$ constructs both in the bound and unbound state. In the published crystal structure of NEMO$_{44-111}$ in complex with IKK$\beta_{701-745}$ electron density could be resolved only for the residues from residues 49 to 110,[16] suggesting that a few additional residues could also be dispensed with. Given the strong correlation between structural order and the prospects for obtaining protein crystals that diffract with high resolution, our results suggest that our shorter, disulfide-stabilized constructs NEMO$_{44-111}$(des2C/C54), NEMO$_{44-111}$(des3C/L107C) and NEMO$_{44-111}$(des2C/C54/L107C), or versions of these constructs that are further truncated to remove a small number of amino acids at the N terminus, are good candidates for crystallization in an unbound state, and for cocrystallization with inhibitors.

■ ASSOCIATED CONTENT

Supporting Information

Results from additional control experiments and data sets obtained for the NEMO$_{44-111}$ constructs, where not shown in the main text. This material is available free of charge via the Internet at http://pubs.acs.org.

■ AUTHOR INFORMATION

Corresponding Authors

*(A.W.) Mailing address: Boston University, Department of Chemistry, 590 Commonwealth Avenue, Boston, MA 02215. Phone: 617-353-2488. E-mail: whitty@bu.edu.

*(T.D.G.) Mailing address: Boston University, Department of Biology, 5 Cummington Mall, Boston, MA 02215. Phone: 617-353-5444. E-mail: gilmore@bu.edu.

*(K.N.A.) Mailing address: Department of Chemistry, 590 Commonwealth Avenue, Boston, MA 02215. Phone: 617-358-5544. E-mail: drkallen@bu.edu.

Funding

This research was supported by NIH Grant GM094551. CB and UW received funding from the Boston University Undergraduate Research Opportunities Program. The CD spectrometer was purchased under NSF grant CHE1126545.

Notes

The authors declare no competing financial interest.

■ ACKNOWLEDGMENTS

We thank Alexander Hoffmann (UCSD) for NEMO-deficient fibroblasts, and Sandor Vajda for helpful discussions. We thank Shi-Yuan Cheng (Northwestern University) for the HA-TRAF6 expression vector.

■ ABBREVIATIONS

CC, the coiled-coil domain of NEMO; CD, circular dichroism; Cys, cysteine; DTT, dithiothreitol; FA, fluorescence anisotropy; HLX1, the first helix region of NEMO; HLX2, the second helix region of NEMO; IκB, inhibitor of kappa-B; IKK, IκB kinase; IPTG, isopropyl β-D-1-thiogalactopyranoside; LB, lysogeny broth, a.k.a. Luria broth; LZ, leucine zipper; NEMO, NF-κB essential modulator; NF-κB, nuclear factor κB; PMSF, phenylmethanesulfonylfluoride; TCEP, 3,3′,3″-phosphanetriyl-tripropanoic acid; SUMO, small ubiquitin-like modifier protein; TEV, tobacco etch virus; TFE, 2,2,2-trifluoroethanol; TNFα, tumor necrosis factor alpha; ZF, zinc finger domain of NEMO

■ REFERENCES

(1) Chu, H. X., Zhu, J. F., Huang, J. J., Jiang, Z. Y., Lu, M. C., Zhang, X. J., Sun, H. P., and You, Q. D. (2014) Insights into targeting NEMO for pharmacological regulation. *Curr. Drug Targets 15*, 874−887.

(2) Carvalho, G., Fabre, C., Braun, T., Grosjean, J., Ades, L., Agou, F., Tasdemir, E., Boehrer, S., Israël, A., Veron, M., Fenaux, P., and Kroemer, G. (2007) Inhibition of NEMO, the regulatory subunit of

the IKK complex, induces apoptosis in high-risk myelodysplastic syndrome and acute myeloid leukemia. *Oncogene 26*, 2299−2307.
(3) Huxford, T., and Ghosh, G. (2009) A structural guide to proteins of the NF-κB signaling module. *Cold Spring Harb. Perspect. Biol. 1*, a000075.
(4) Oeckinghaus, A., and Ghosh, S. (2009) The NF-κB family of transcription factors and its regulation. *Cold Spring Harbor Perspect. Biol. 1*, a000034.
(5) Tak, P. P., and Firestein, G. S. (2001) NF-κB: A key role in inflammatory diseases. *J. Clin. Invest. 107*, 7−11.
(6) Dolcet, X., Llobet, D., Pallares, J., and Matias-Guiu, X. (2005) NF-κB in development and progression of human cancer. *Virchows Arch. 446*, 475−482.
(7) May, M. J., D'Acquisto, F., Madge, L. A., Glöckner, J., Pober, J. S., and Ghosh, S. (2000) Selective inhibition of NF-κB activation by a peptide that blocks the interaction of NEMO with the IκB kinase complex. *Science 289*, 1550−1554.
(8) Strickland, I., and Ghosh, S. (2006) Use of cell permeable NBD peptides for suppression of inflammation. *Ann. Rheum. Dis. 65* (Suppl 3), iii75−82.
(9) Yang, D., Sun, Y. Y., Lin, X., Baumann, J. M., Dunn, R. S., Lindquist, D. M., and Kuan, C. Y. (2013) Intranasal delivery of cell-penetrating anti-NF-κB peptides (tat-NBD) alleviates infection-sensitized hypoxic-ischemic brain injury. *Exp. Neurol. 247*, 447−455.
(10) von Bismarck, P., Winoto-Morbach, S., Herzberg, M., Uhlig, U., Schutze, S., Lucius, R., and Krause, M. F. (2012) IKK NBD peptide inhibits LPS induced pulmonary inflammation and alters sphingolipid metabolism in a murine model. *Pulm. Pharmacol. Ther. 25*, 228−235.
(11) Fabrice Agou, F. Y., Goffinont, S., Courtois, G., Yamaoka, S., Israël, A., and Véron, M. (2002) NEMO trimerizes through its coiled-coil C-terminal domain. *J. Biol. Chem. 277*, 17464−17475.
(12) Lo, Y. C., Maddineni, U., Chung, J. Y., Rich, R. L., Myszka, D. G., and Wu, H. (2008) High-affinity interaction between IKKβ and NEMO. *Biochemistry 47*, 3109−3116.
(13) Agou, F., Traincard, F., Vinolo, E., Courtois, G., Yamaoka, S., Israël, A., and Veron, M. (2004) The trimerization domain of NEMO is composed of the interacting C-terminal CC2 and LZ coiled-coil subdomains. *J. Biol. Chem. 279*, 27861−27869.
(14) Ivins, F. J., Montgomery, M. G., Smith, S. J., Morris-Davies, A. C., Taylor, I. A., and Rittinger, K. (2009) NEMO oligomerization and its ubiquitin-binding properties. *Biochem. J. 421*, 243−251.
(15) Cote, S. M., Gilmore, T. D., Shaffer, R., Weber, U., Bollam, R., Golden, M. S., Glover, K., Herscovitch, M., Ennis, T., Allen, K. N., and Whitty, A. (2013) Mutation of nonessential cysteines shows that the NF-κB essential modulator forms a constitutive noncovalent dimer that binds IκB kinase-β with high affinity. *Biochemistry 52*, 9141−9154.
(16) Rushe, M., Silvian, L., Bixler, S., Chen, L. L., Cheung, A., Bowes, S., Cuervo, H., Berkowitz, S., Zheng, T., Guckian, K., Pellegrini, M., and Lugovskoy, A. (2008) Structure of a NEMO/IKK-associating domain reveals architecture of the interaction site. *Structure 16*, 798−808.
(17) Zheng, C., Yin, Q., and Wu, H. (2011) Structural studies of NF-κB signaling. *Cell Res. 21*, 183−195.
(18) Shifera, A. S. (2010) Protein-protein interactions involving IKKγ (NEMO) that promote the activation of NF-κB. *J. Cell. Physiol. 223*, 558−561.
(19) Shifera, A. S. (2010) Proteins that bind to IKKγ (NEMO) and down-regulate the activation of NF-κB. *Biochem. Biophys. Res. Commun. 396*, 585−589.
(20) Claire Bagnéris, A. V. A., Cronin, N., Wallace, B., Collins, M., Boshoff, C., Waksman, G., and Barrett, T. (2008) Crystal structure of a vFLIP-IKKγ complex: Insights into viral activation of the IKK signalosome. *Mol. Cell 30*, 620−631.
(21) Yoshikawa, A., Sato, Y., Yamashita, M., Mimura, H., Yamagata, A., and Fukai, S. (2009) Crystal structure of the NEMO ubiquitin-binding domain in complex with Lys 63-linked di-ubiquitin. *FEBS Lett. 583*, 3317−3322.
(22) Golden, M. S., Cote, S. M., Sayeg, M., Zerbe, B. S., Villar, E. A., Beglov, D., Sazinsky, S. L., Georgiadis, R. M., Vajda, S., Kozakov, D., and Whitty, A. (2013) Comprehensive experimental and computational analysis of binding energy hot spots at the NF-κB essential modulator/IKKβbeta protein-protein interface. *J. Am. Chem. Soc. 135*, 6242−6256.
(23) Whitty, A., and Kumaravel, G. (2006) Between a rock and a hard place? *Nat. Chem. Biol. 2*, 112−118.
(24) Wells, J. A., and McClendon, C. L. (2007) Reaching for high-hanging fruit in drug discovery at protein-protein interfaces. *Nature 450*, 1001−1009.
(25) Fauman, E. B., Rai, B. K., and Huang, E. S. (2011) Structure-based druggability assessment—Identifying suitable targets for small molecule therapeutics. *Curr. Opin. Chem. Biol. 15*, 463−468.
(26) Hajduk, P. J., Huth, J. R., and Fesik, S. W. (2005) Druggability indices for protein targets derived from NMR-based screening data. *J. Med. Chem. 48*, 2518−2525.
(27) Wanner, J., Fry, D. C., Peng, Z., and Roberts, J. (2011) Druggability assessment of protein-protein interfaces. *Future Med. Chem. 3*, 2021−2038.
(28) Herscovitch, M., Comb, W., Ennis, T., Coleman, K., Yong, S., Armstead, B., Kalaitzidis, D., Chandani, S., and Gilmore, T. D. (2008) Intermolecular disulfide bond formation in the NEMO dimer requires Cys54 and Cys347. *Biochem. Biophys. Res. Commun. 367*, 103−108.
(29) Feng, H., Lopez, G. Y., Kim, C. K., Alvarez, A., Duncan, C. G., Nishikawa, R., Nagane, M., Su, A. J., Auron, P. E., Hedberg, M. L., Wang, L., Raizer, J. J., Kessler, J. A., Parsa, A. T., Gao, W. Q., Kim, S. H., Minata, M., Nakano, I., Grandis, J. R., McLendon, R. E., Bigner, D. D., Lin, H. K., Furnari, F. B., Cavenee, W. K., Hu, B., Yan, H., and Cheng, S. Y. (2014) EGFR phosphorylation of DCBLD2 recruits TRAF6 and stimulates Akt-promoted tumorigenesis. *J. Clin. Invest. 124*, 3741−3756.
(30) Walker, J., Gasteiger, E., Hoogland, C., Gattiker, A., Duvaud, S. E., Wilkins, M., Appel, R., and Bairoch, A. (2005) Protein identification and analysis tools on the ExPASy server. In *The Proteomics Protocols Handbook* (Walker, J., Ed.), pp 571−607, Humana Press, New York.
(31) Parks, T. D., Leuther, K. K., Howard, E. D., Johnston, S. A., and Dougherty, W. G. (1994) Release of proteins and peptides from fusion proteins using a recombinant plant virus proteinase. *Anal. Biochem. 216*, 413−417.
(32) Anthis, N. J., and Clore, G. M. (2013) Sequence-specific determination of protein and peptide concentrations by absorbance at 205 nm. *Protein Sci. 22*, 851−858.
(33) Day, E. S., Wen, D., Garber, E. A., Hong, J., Avedissian, L. S., Rayhorn, P., Shen, W., Zeng, C., Bailey, V. R., Reilly, J. O., Roden, J. A., Moore, C. B., Williams, K. P., Galdes, A., Whitty, A., and Baker, D. P. (1999) Zinc-dependent structural stability of human sonic hedgehog. *Biochemistry 38*, 14868−14880.
(34) Pace, C. N. (1990) Measuring and increasing protein stability. *Trends Biotechnol. 8*, 93−98.
(35) Hazes, B., and Dijkstra, B. W. (1988) Model building of disulfide bonds in proteins with known three-dimensional structure. *Protein Eng. 2*, 119−125.
(36) Luidens, M. K., Figge, J., Breese, K., and Vajda, S. (1996) Predicted and trifluoroethanol-induced alpha-helicity of polypeptides. *Biopolymers 39*, 367−376.
(37) Luo, P., and Baldwin, R. L. (1997) Mechanism of helix induction by trifluoroethanol: A framework for extrapolating the helix-forming properties of peptides from trifluoroethanol/water mixtures back to water. *Biochemistry 36*, 8413−8421.
(38) Roehrl, M. H., Wang, J. Y., and Wagner, G. (2004) A general framework for development and data analysis of competitive high-throughput screens for small-molecule inhibitors of protein-protein interactions by fluorescence polarization. *Biochemistry 43*, 16056−16066.
(39) Greenfield, N. J. (2007) Using circular dichroism spectra to estimate protein secondary structure. *Nat. Protoc. 1*, 2876−2890.
(40) Gautheron, J., and Courtois, G. (2010) "Without Ub I am nothing": NEMO as a multifunctional player in ubiquitin-mediated control of NF-κB activation. *Cell. Mol. Life Sci. 67*, 3101−3113.

(41) Schrofelbauer, B., Polley, S., Behar, M., Ghosh, G., and Hoffmann, A. (2012) NEMO ensures signaling specificity of the pleiotropic IKKβ by directing its kinase activity toward IκBα. *Mol. Cell 47*, 111−121.
(42) Rahighi, S., Ikeda, F., Kawasaki, M., Akutsu, M., Suzuki, N., Kato, R., Kensche, T., Uejima, T., Bloor, S., Komander, D., Randow, F., Wakatsuki, S., and Dikic, I. (2009) Specific recognition of linear ubiquitin chains by NEMO is important for NF-κB activation. *Cell 136*, 1098−1109.
(43) Sebban-Benin, H., Pescatore, A., Fusco, F., Pascuale, V., Gautheron, J., Yamaoka, S., Moncla, A., Ursini, M. V., and Courtois, G. (2007) Identification of TRAF6-dependent NEMO polyubiquitination sites through analysis of a new NEMO mutation causing incontinentia pigmenti. *Hum. Mol. Genet. 16*, 2805−2815.
(44) Gautheron, J., Pescatore, A., Fusco, F., Esposito, E., Yamaoka, S., Agou, F., Ursini, M. V., and Courtois, G. (2010) Identification of a new NEMO/TRAF6 interface affected in incontinentia pigmenti pathology. *Hum. Mol. Genet. 19*, 3138−3149.
(45) Tanford, C. (1964) Isothermal unfolding of globular proteins in aqueous urea solutions. *J. Am. Chem. Soc. 86*, 2050−2059.
(46) Scholtz, J. M., Grimsley, G. R., and Pace, C. N. (2009) Solvent denaturation of proteins and interpretations of the *m* value. *Methods Enzymol. 466*, 549−565.
(47) Shortle, D. (1995) Staphylococcal nuclease: A showcase of *m*-value effects. *Adv. Prot. Chem. 46*, 217−247.
(48) Page, M. I., and Jencks, W. P. (1971) Entropic contributions to rate accelerations in enzymic and intramolecular reactions and the chelate effect. *Proc. Natl. Acad. Sci. U. S. A. 68*, 1678−1683.
(49) Chang, C. E., McLaughlin, W. A., Baron, R., Wang, W., and McCammon, J. A. (2008) Entropic contributions and the influence of the hydrophobic environment in promiscuous protein-protein association. *Proc. Natl. Acad. Sci. U. S. A. 105*, 7456−7461.
(50) Lundquist, J. J., and Toone, E. J. (2002) The cluster glycoside effect. *Chem. Rev. 102*, 555−578.
(51) Lazaridis, T., Masunov, A., and Gandolfo, F. (2002) Contributions to the binding free energy of ligands to avidin and streptavidin. *Proteins 47*, 194−208.
(52) Finkelstein, A. V., and Janin, J. (1989) The price of lost freedom: Entropy of bimolecular complex formation. *Protein Eng. 3*, 1−3.
(53) Day, E. S., Cote, S. M., and Whitty, A. (2012) Binding efficiency of protein-protein complexes. *Biochemistry 51*, 9124−9136.
(54) May, M. J., Marienfeld, R. B., and Ghosh, S. (2002) Characterization of the IκB-kinase NEMO binding domain. *J. Biol. Chem. 277*, 45992−46000.
(55) Baima, E. T., Guzova, J. A., Mathialagan, S., Nagiec, E. E., Hardy, M. M., Song, L. R., Bonar, S. L., Weinberg, R. A., Selness, S. R., Woodard, S. S., Chrencik, J., Hood, W. F., Schindler, J. F., Kishore, N., and Mbalaviele, G. (2010) Novel insights into the cellular mechanisms of the anti-inflammatory effects of NF-κB essential modulator binding domain peptides. *J. Biol. Chem. 285*, 13498−13506.
(56) Gotoh, Y., Nagata, H., Kase, H., Shimonishi, M., and Ido, M. (2010) A homogeneous time-resolved fluorescence-based high-throughput screening system for discovery of inhibitors of IKKβ-NEMO interaction. *Anal. Biochem. 405*, 19−27.
(57) Courtois, G., and Gilmore, T. D. (2006) Mutations in the NF-κB signaling pathway: Implications for human disease. *Oncogene 25*, 6831−6843.
(58) Florence Cordier, E. V., Véron, M., Delepierre, M., and Agou, F. (2008) Solution structure of NEMO zinc finger and impact of an anhidrotic ectodermal dysplasia with immunodeficiency-related point mutation. *J. Mol. Biol. 377*, 1419−1432.
(59) Creighton, T. E. (1988) Disulphide bonds and protein stability. *BioEssays 8*, 57−63.